

# COHERENT OPTICAL TECHNIQUES FOR THE ANALYSIS OF TISSUE STRUCTURE AND DYNAMICS

Valery V. Tuchin

Saratov State University, Optics Department, 83 Astrakhanskaya, Saratov 410026, Russia

(Paper CDO-005 received Oct. 20, 1997; revised manuscript received Nov. 23, 1998; accepted for publication Nov. 23, 1998.)

## ABSTRACT

This paper summarizes the description of the speckle-correlation, speckle-interferometric, and polarimetric methods and instruments designed for various tissue structure imaging and their optical and dynamical parameter monitoring. © 1999 Society of Photo-Optical Instrumentation Engineers. [S1083-3668(99)01201-0]

**Keywords** speckles; interferometry; scattering; tissue; blood; lymph.

## 1 INTRODUCTION

At present a number of optical technologies for tissue structure and dynamics analysis are available. Many of them are based on detection of photon diffusion in continuous wave (cw), time-domain, and frequency-domain modes.<sup>1,2</sup> Recently the coherence-domain and polarimetric methods were shown to be a more simple and robust alternative for noncoherent photon diffusion methods and ultrashort pulse techniques, when applied for rather thin tissues.<sup>1–11</sup> Such methods are based on coherent or polarized light interaction with a scattering medium. Speckle optics and speckle interferometry,<sup>2,3,12–24</sup> dynamic light scattering,<sup>25–33</sup> interferometry,<sup>34,35</sup> diffractometry,<sup>36,37</sup> optical heterodyning,<sup>1,38–41</sup> phase, confocal and holographic microscopy,<sup>3,39,42–52</sup> diffusing wave spectroscopy and interferometry,<sup>53–57</sup> low coherence interferometry,<sup>1,3,4,58–62</sup> as well as Mueller matrix measurement methods<sup>3,5,63–67</sup> belong to coherent and polarimetric technologies which are very promising for tissue and cell structure, optical and dynamical parameter monitoring.

This article concentrates on the analysis of certain coherent and polarimetric methods and instruments recently designed for tissue and cell structure and motion imaging and monitoring by the biomedical optics group of Saratov Scientific Center in Russia. Many other directions of optical speckle and polarimetric technologies for biomedicine, coherent interferometry and tomography, confocal

and phase microscopy are discussed well in recent review articles and books.<sup>1–4,12,13,15,28,34,43–46,58–64,67,68</sup>

## 2 OPTICAL SPATIAL SPECKLE-CORRELOMETRY TECHNIQUE FOR TISSUE STRUCTURE IMAGING AND MONITORING

### 2.1 PRINCIPLES OF THE TECHNIQUE

The fine structure of the scattering light patterns formed as a result of the coherent illumination of a turbid media contains information about its structure (morphology). Unfortunately, this information is hidden in the scattered field spatial-temporal distributions (statistical and correlation characteristics of intensity fluctuations, state of polarization, etc). That is why the main problem of the coherent light imaging and tomography is displaying of inner structure of the object using the analysis of such patterns. Living tissues are characterized by the complex hierarchy of structure organization which does not allow us as a rule to build an adequate scattering model needed for complete tomographic reconstruction.<sup>1,2</sup> Nevertheless, such reconstruction can be successfully replaced by a generalized description of the statistical and correlation properties of the object (probability density function of inhomogeneities sizes and refractive index distributions or corresponding statistical moments, e.g., mean size and size dispersion, etc).

To describe statistical properties of the scattered light intensity fluctuations two general parameters are usually introduced:<sup>69,70</sup> mean intensity value in the observation point  $\langle I \rangle$  and the second-order statistical moment (variance) of intensity fluctuations

This paper was written on the basis of the overview by V. V. Tuchin: "Coherent and polarimetric optical technologies for analysis of tissue structure," *Proc. SPIE* **2981**, 120–159 (1997).

Address all correspondence to Valery V. Tuchin. Laboratory of Laser Diagnostics of Technical and Living Systems, Precision Mechanics and Control Institute of the Russian Academy of Sciences, 24 Rabochaya, Saratov 410028, Russia. Tel: (8452) 29-16-93; Fax: (8452) 24-04-46; E-mail: tuchin@sgu.ssu.runnet.ru

$\sigma_I^2 = \langle (I - \langle I \rangle)^2 \rangle$ , its normalized value is the speckle contrast

$$V = \sigma_I / \langle I \rangle. \quad (1)$$

In addition, the normalized third-order moment can be included into this set of parameters

$$Q_a = \langle (I - \langle I \rangle)^3 \rangle / [\langle (I - \langle I \rangle)^2 \rangle]^{1.5}. \quad (2)$$

Parameter  $Q_a$  evaluates the degree of skewness of the intensity statistical distributions and can be used as an indicator of probability density functions (PDFs) tails existence. These first-order statistical properties can be examined as a "single point," or statistical itself, parameters.

To describe correlation properties of spatial distributions of intensity fluctuations caused by the sample scanning "two-point" statistical parameters such as correlation function  $R_I$  and structure function  $D_I$  must be introduced:<sup>3,69,70</sup>

$$R_I(\Delta \vec{\rho}) = \langle [I(\vec{\rho} + \Delta \vec{\rho}) - \langle I \rangle][I(\vec{\rho}) - \langle I \rangle] \rangle, \quad (3)$$

$$D_I(\Delta \vec{\rho}) = \langle [I(\vec{\rho} + \Delta \vec{\rho}) - I(\vec{\rho})]^2 \rangle,$$

$$D_I(\Delta \vec{\rho}) = 2[R_I(0) - R_I(\Delta \vec{\rho})].$$

Isotropic and statistically homogeneous scattering structures  $R_I(\Delta \vec{\rho})$  and  $D_I(\Delta \vec{\rho})$  depend only on argument module  $|\Delta \vec{\rho}|$ ,  $\vec{\rho} = (x, y)$ . To simplify the structure analysis a normalized autocorrelation function  $r_I(\Delta \vec{\rho}) = R_I(\Delta \vec{\rho}) / R_I(0)$  is usually used.  $R_I(\Delta \vec{\rho})$  and  $r_I(\Delta \vec{\rho})$  are more preferable for analysis of intensity fluctuations caused by the large inhomogeneities of the object.  $D_I(\Delta \vec{\rho})$  is more sensitive to the small-scale intensity oscillations as well.

Behavior of  $D_I(\Delta \vec{\rho})$  in the vicinity of zero value of its argument is defined by the high frequency spatial intensity fluctuations and can be described by the value of the exponential factor  $\nu_I$ ,

$$\nu_I = \ln[D_I(\Delta \vec{\rho}_2) / D_I(\Delta \vec{\rho}_1)] / \ln(|\Delta \vec{\rho}_2| / |\Delta \vec{\rho}_1|), \quad (4)$$

which for isotropic scalar distributions is directly connected with their fractal or Hausdorff-Besicovitch dimension  $D_{HB}$ .<sup>71</sup>

$$\nu_I = 2(2 - D_{HB}). \quad (5)$$

Here  $D_{HB}$  changes between 1 and 2 and describe properties of the arbitrary selected one-dimensional section of the corresponding two-dimensional (2D) distribution, for the "conventional" differentiated scalar isotropic distributions, so-called marginal fractals:  $D_{HB} = 1$ ,  $\nu = 2$ ; for Brownian fractals:  $D_{HB} = 1.5$ ,  $\nu = 1$ ; and for extreme fractals:  $D_{HB} = 2$ ,  $\nu = 0$ .

The scalar diffraction theory of far-zone speckle pattern formation for diffraction of a broad collimated beam on a random phase screen allows us to obtain<sup>3</sup>

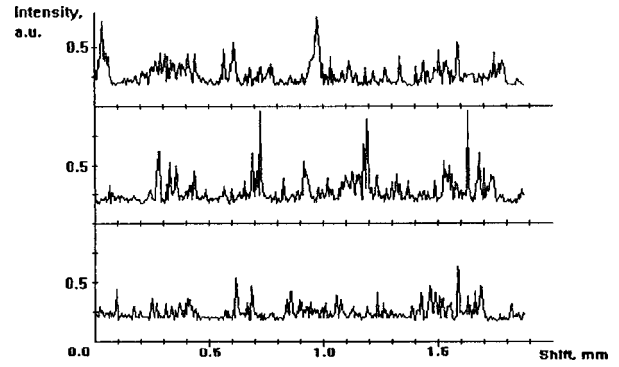


**Fig. 1** The time series of speckle intensity fluctuation induced by the sample (psoriatic human skin epidermis stripping) scanning. Upper and lower traces are measured for a sample surface tuned out of the beam waist plane (correspondingly focused in front of and beyond the sample surface); mid is measured for the sample surface tuned to the beam waist plane.

$$D_I(\Delta \vec{\rho}) = \exp[-D_\phi(\Delta \vec{\rho})], \quad (6)$$

$$\nu_I = \nu_\phi,$$

where  $D_\phi(\Delta \vec{\rho})$  and  $\nu_\phi$  are the structure function and corresponding exponential factor of the phase fluctuations of the boundary field.

For strongly focused light beam diffraction a more complicated relationship between  $\nu_I(D_{HB}^I)$  and  $\nu_\phi(D_{HB}^\phi)$  is expected.<sup>3</sup> In particular, for  $\nu_\phi < 2$  (respectively,  $D_{HB}^\phi > 1$ ) the spatial power spectrum of the phase fluctuations contains the high frequency components,  $\nu_I < \nu_\phi$ , and  $D_{HB}^I > D_{HB}^\phi$ .

Speckle pattern local statistical and correlation analysis is very promising for 2D imaging ("mapping") and monitoring of the scattering structures.<sup>3,72-81</sup> The local estimations of generalized correlation characteristics (such as the exponential factor  $\nu_I$ ) as well as normalized statistical moments (contrast  $V$  and skewness coefficient  $Q_a$  are usually used) show the strong dependence on structure parameters of the object [such as correlation length  $l_h$  and root mean square (rms) value  $\sigma_h$  of optical heights of inhomogeneities or corresponding correlation length  $l_\phi$  and rms value  $\sigma_\phi$  of phase fluctuations of the boundary field] if focused illuminating beams are used. The object under investigation can be considered as an irregular set of "microlenses" with certain statistical characteristics which produces corresponding intensity fluctuations while the focused laser beam is scanning.<sup>76,80</sup> Intensity fluctuation signal is the combination of two components (see Figure 1): relatively low amplitude and smooth-varying background and rare appearing high-amplitude pulses. The last ones caused by the "matched" inhomogeneities when distances between illuminating beam waist plane and object and between object and detector are

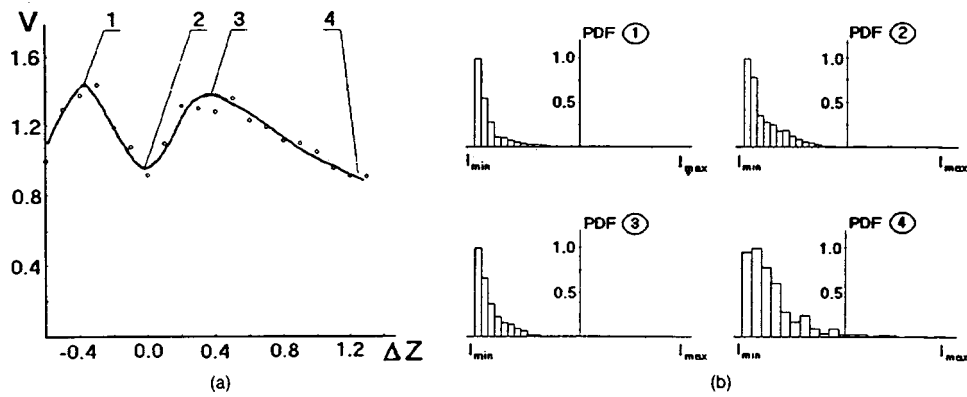


**Fig. 2** The relation between the contrast values (a) and view of experimental probability density function (PDF) (b) for various  $\Delta z$  (mm) values.  $\Delta z$  is the distance between the focused beam waist position and the sample surface; the  $\Delta z=0$  position corresponds to the sample surface just in the beam waist plane. The sample is the epidermal stripping of the human psoriatic skin.

matched with the inhomogeneity effective focal length to provide beam waist image formation in the observation plane.

Inhomogeneity classification can be carried out by the analysis of the dependence of contrast  $V$  and skewness coefficient  $Q_a$  on the distance between the beam waist plane and the sample surface: in such a way, statistical distributions of refractive index fluctuations can be reconstructed.<sup>79</sup> The sharp increase of  $V$  and  $Q_a$  for the illuminating beam radius  $w \sim l_\phi$  is the direct manifestation of the “microfocusing” effect in the far diffraction zone<sup>76,80</sup> (see Figure 2 for  $V$ ,  $\Delta z = \pm 0.4$  mm). The increase of  $w/l_\phi$  ratio ( $|\Delta z| > 0.4$  mm) is accompanied by the gradual decrease of  $V$  and  $Q_a$  to values characteristic for the fully developed speckle patterns ( $V = 1$  and  $Q_a = 2$ ).

For weak scattering objects, like a thin tissue layer  $l_h \sim l_\phi \sim l$  ( $l$  is the tissue sample thickness,  $l_h \gg \lambda$ ,  $\lambda$  is the wavelength), the rms values of phase fluctuations  $\sigma_\phi$  are directly connected to refractive index fluctuations  $\delta n$ . On the contrary, for the optically thick tissue layers multiple scattering is typical, the broad angular spectrum of the scattered light took place, and depolarization effects are significant. For the generalized characterization of tissue scattering structure the following set of parameters are usually used: absorption and scattering coefficients  $\mu_a$  and  $\mu_s$ ,  $\mu_s \gg \mu_a$ , reduced scattering coefficient  $\mu'_s = \mu_s(1-g)$ , where  $g$  is the scattering anisotropy factor, and photon transport mean free path  $l^* \sim 1/(\mu_a + \mu'_s)$  as well as the most probable photon path length  $s \sim l^2/l^*$ .<sup>54</sup> As a rule, the decrease of inhomogeneity size  $l_h$  and rise of refractive index fluctuations  $\delta n$  is accompanied by strong scattering; ratio  $l/l_h$  becomes much greater than unity. Analysis of temporal autocorrelation functions of the scattered light intensity fluctuations induced by a fluctuating turbid media is the basis of diffusing-wave spectroscopy (DWS) which allows us to provide new fundamental information about

motion and structure of tissue and its dynamical properties.<sup>53-57</sup> The normalized intensity autocorrelation function  $\tilde{g}_2(\tau)$  can be presented as

$$\tilde{g}_2(\tau) = \langle \tilde{I}(t)\tilde{I}(t+\tau) \rangle / \langle \tilde{I}^2(t) \rangle, \quad (7)$$

where  $\tilde{I}(t) = I(t) - \langle I(t) \rangle$ . This temporal function is defined by the scanning velocity of the laser beam used, its beam waist radius, and spatial fluctuations of the media under investigation.<sup>73</sup>

The multiple scattering is accompanied by changes of the initial polarization state of the probe beam that can be described using the correlation analysis of the scattered light components with different polarization states. The following time-dependent first- and second-order statistical characteristics of the scattered light intensity fluctuations in the paraxial region can be studied experimentally for two different linear polarization states  $\parallel$  and  $\perp$  (in respect to the state of polarization of the probe beam).

The mean intensity of speckles

$$\langle I_s \rangle = \langle I_\parallel \rangle + \langle I_\perp \rangle, \quad (8)$$

and the cross-correlation function (correlation coefficient) for both polarization states

$$r_{\perp\parallel}(\tau) = \langle [I_\parallel(t) - \langle I_\parallel \rangle][I_\perp(t+\tau) - \langle I_\perp \rangle] \rangle, \quad (9)$$

where the pair of subscripts ( $\perp, \parallel$ ) denotes the combinations of polarization states. The averaging is carried out along the scanning trace length.

The optical scheme of the spatial speckle-correlometer is shown in Figure 3. The illuminating laser beam with  $\lambda = 633$  nm focused up to a spot of about  $5 \mu\text{m}$  was used. In general, for image reconstruction of the object structure two-dimensional scanning was performed and corresponding analysis of the statistical and correlation properties of the scattered light was carried out. Scanning steps for both dimensions were equal to  $5 \mu\text{m}$ . An on-axis position of the photodetector corresponding to zero

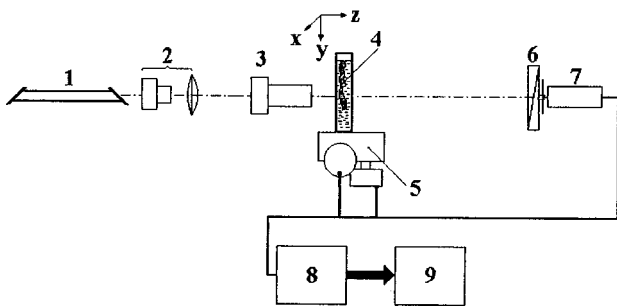


**Fig. 3** Optical scheme of the scanning polarization sensitive spatial speckle correlometer: 1—monomode He–Ne laser (633 nm, 2 mW) with linear polarization of its radiation; 2—telescope; 3—focusing micro-objective; 4—tissue under study; 5—computer controlled 2D-scanning device; 6—manually rotating polarizer; 7—photomultiplier with a pinhole; 8—analog-to-digital converter; 9—PC.

scattering angle was used; the pinhole diameter (about  $25\ \mu\text{m}$ ) was much less than the speckle average size. The ratio of driving frequency (used for control of stepper motors of the 2D-scanning device) to sampling frequency of the analog-to-digital converter of the intensity detection channel allows us to obtain a sampling interval equal to  $5 \times 10^{-5}$  s or less. For scanning velocity equal to 5 mm/s the electronics used allowed us to obtain at least 20 equidistant sampling points per one scanning step, i.e., spatial resolution of about  $0.25\ \mu\text{m}$  was provided. Samples under study were usually placed in the waist plane of the illuminating beam; the position of the sample with respect to beam waist plane was adjusted manually. Manually rotating the polarizer between the sample and photodetector provided polarization measurements of intensity fluctuations of the scattered light.

## 2.2 THE HUMAN SKIN INVESTIGATION

In general, for estimation of tissue structure parameters, such as characteristic size of local inhomogeneities and refractive index spatial fluctuations, the model of scattering structure should be assumed. The simplest one is the model of Gaussian random phase screen.<sup>69,70,75,81</sup> Indeed, statistical models of living structures should be more complicated, in particular, nonlinear ones accounting for multiple scattering. In spite of the lack of developed tissue structure models any empirical information about statistical properties of the scattered light should be valuable for tissue structure imaging analysis as well as for development of these models.

Human skin is one of the most evident objects for optical spatial speckle correlometry.<sup>3,73–77,79</sup> All structural peculiarities of the skin are displayed in statistical and correlation properties of the far-zone speckles produced by the focused beam illumination of skin samples or its replicas. Glass-glue epidermal stripping technology is very suitable for providing *in vitro* spectrophotometric, fluorescence, and correlation measurements.<sup>75,82</sup> Such a stripping

sample is a thin epidermal layer (about  $30\text{--}50\ \mu\text{m}$  in thickness) attached to a high-quality glass plate. The detected time series of intensity fluctuations of the focused laser beam transmitted through the epidermal sample of the psoriatic skin is presented in Figure 1. The intensity fluctuations are caused by the sample scanning across the light beam. Thin layers of normal and psoriatic epidermis investigated showed rather weak scattering (single or low step), because the measured degree of depolarization of the scattered light in the far field was very weak.

The dependencies of contrast  $V$  and skewness coefficient  $Q_a$  of the far-zone speckle intensity fluctuations on the defocusing parameter  $\Delta z$  for normal and psoriatic epidermis show two maxima around the position of the sample front surface strictly in the beam waist ( $\Delta z = 0$ ).<sup>76</sup> For the psoriatic skin sample such dependence for contrast and corresponding PDFs are presented in Figure 2. The presented first-order statistical characteristics confirm the validity of a “lens-let” approach for the description of scattering properties of the thin layers of human epidermis. For normal epidermis (fewer sizes of scatterers and a more homogeneous scattering structure are characteristic) partial overlapping of both maxima (at least for small magnification of focusing microobjective) was observed. Symmetry of  $V$  or  $Q_a$  peak positions with respect to the waist plane allows us to propose the equality of statistical weights of “negative” and “positive” “microlenses” within the ensemble of local scatterers.

Differences between  $V(\Delta z)$  and  $Q_a(\Delta z)$  curves for normal and psoriatic epidermis samples are caused by tissue structure changes as a result of disease progression. These changes arise due to appearance of parakeratosis focuses (cellular structure within focuses is strongly disordered) and impregnation of surrounding tissue by serum and other tissue fluids (which act as immersion liquids). For later stages of the disease formation of microspaces filled up by air and appearance of superficial skin scales are characteristic;<sup>82</sup> as a result, an increase of light scattering is observed. For small  $\Delta z$  contrast  $V$  exceeds unity and can reach values of about 1.6–1.7 for the individual samples. As a rule, normal skin samples demonstrate larger contrast than the psoriatic ones. The plots for  $\ln Q_a$  versus  $\ln V$  for various  $\Delta z$  illustrate the discrepancy of statistical properties of normal and psoriatic skin samples (see Figure 4): for normal skin the first derivative of  $\ln Q_a = f(\ln V)$  is larger than for the psoriatic one with a negative slope for normal skin and a positive one for pathological. For the fully developed speckle fields with  $V=1$  and negative exponential intensity PDF  $Q_a = 2$ ,<sup>83</sup> the corresponding points are shown by the sign +. Discussed first-order statistics measurements can serve as a simple and effective criterion for human skin structure recognition. It can also be

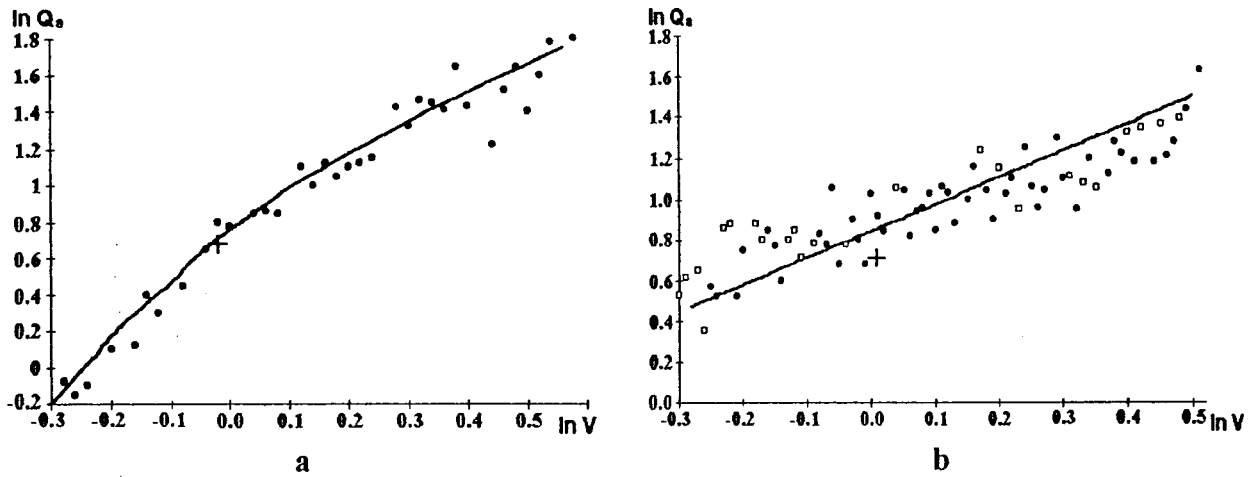


**Fig. 4** Functions of  $\ln Q_o$  vs  $\ln V$  measured for the human skin epidermal strippings for various values of defocusing parameter  $\Delta z$ : (a) normal skin (two samples); (b) psoriatic skin (two samples). + denotes  $Q_o$  and  $V$  values for fully developed speckles.

used for analysis of the replicas of the human skin.<sup>77</sup> For example, skin replicas obtained by application of D-SQUAME<sup>®</sup> disks are usually used for rapid semiquantitative estimation of skin dryness or oiliness. The speckle statistics technique allows us to describe the skin properties more precisely and objectively. The experimental data presented in Table 1 illustrate the sensitivity of a speckle technique.

The second-order statistics, or correlation characteristics, of speckle intensity fluctuations show a high sensitivity to discussed changes in tissue structure.<sup>75</sup> For normal skin the normalized 1D intensity autocorrelation functions demonstrate a relatively small value of correlation length  $l_I \sim 60\text{--}80 \mu\text{m}$  and the absence of significant fluctuations of the correlation coefficient in the large-scale region (see Figure 5). With formation of the psoriatic plaque autocorrelation functions show an approximate  $2\times$  increase of the correlation length,  $l_I \sim 95\text{--}180 \mu\text{m}$ , and the presence of relatively large-amplitude and large-scale aperiodical oscillations; effective sizes of the structure inhomogeneities producing such oscillations are correlated with the ones for the parakeratosis focuses ensemble. The detailed analysis of the oscillation components of

the intensity autocorrelation function will allow for estimation the parakeratosis focuses surface density and their mean size.

In the small-scale region for spatial frequencies about  $1 \mu\text{m}^{-1}$  and more, the structure function is more appropriate for characteristic of intensity fluctuations [see Eq. (3)]. The local estimations of exponential factor  $\nu_I$  [see Eq. (4)] allow us to evaluate such fluctuations caused by the high-frequency components of tissue structure and to find their spatial distributions ("maps"). Figure 6 demonstrates such a mapping technique in application to the human epidermal stripping samples of normal and psoriatic skin.<sup>3,74,77,84</sup> All 2D images were obtained using XY scanning of the sample and the focused probing laser beam. Averaging of  $\nu_I$  values had been carried out along the X direction. The size of sampling window used for averaging was not less than  $10^3$  sampling steps; a 16-gradation gray-level scale was used to display 2D distributions of

**Table 1** Contrast  $V$  and coefficient of asymmetry  $Q_o$  values via human skin dryness indices (1  $\rightarrow$  4 dryness increase);  $R = \pi w^2 / \lambda$ ,  $w$  is the waist beam radius. Samples under study—D-SQUAME<sup>®</sup> instant testers (Cu Derm Corp., USA).

Index of dryness	$V$ ( $R=80$ $\mu\text{m}$ )	$V$ ( $R=16$ $\mu\text{m}$ )	$Q_o$ ( $R=80$ $\mu\text{m}$ )	$Q_o$ ( $R=16$ $\mu\text{m}$ )
1	1.126	0.918	1.730	1.110
2	0.925	0.806	1.061	0.479
4	0.692	0.639	0.462	0.122

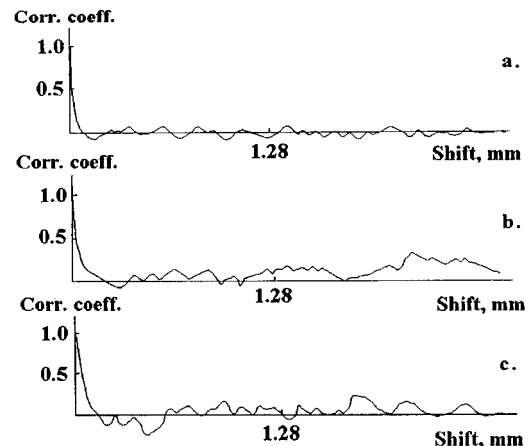


**Fig. 5** Normalized autocorrelation function of the speckle intensity fluctuations measured for a of sample of normal (a) and two samples of psoriatic epidermis (b), (c).

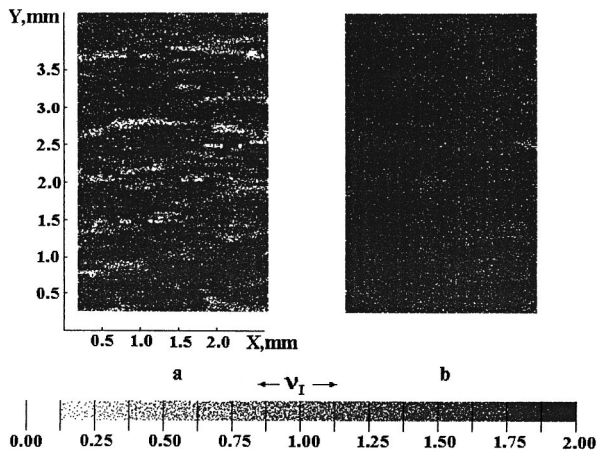


**Fig. 6** 2D maps of exponential factor  $\nu_I$  for the human skin epidermis stripping samples: (a) normal skin; (b) psoriatic skin (middle stage of disease).

$\nu_I$ . Obtained 2D maps and corresponding  $\nu_I$  value distributions (Figures 6 and 7) illustrate stages of disease development. Normal epidermal stripping with relatively small-scale local scattering inhomogeneities is characterized by a slightly smaller mean value and larger dispersion of  $\nu_I$  [Figures 6(a) and 7(a)] in comparison with the early and middle stages of psoriatic plaque formation [Figures 6(b), 7(b), and 7(c)]; large-scale structure peculiarities such as fragments of grid of furrows are clearly manifested in the 2D map. The later stage of psoriatic plaque formation (so-called "desquamation" stage) is characterized by the dispersion and the relatively small mean value of  $\nu_I$  caused by tissue structure transformation (formation of skin scales and microspaces filled up with air).<sup>3,74,77,84</sup>

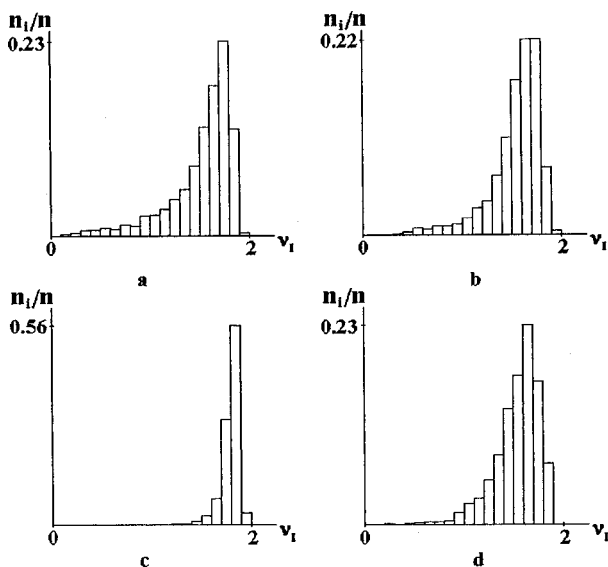


**Fig. 7** Evolution of distributions of exponential factor,  $\nu_I$ , with the psoriasis progression for samples in Figure 6: (a) normal skin; (b), (c), (d) psoriatic skin (three successive stages of disease: early, middle, and later).

### 2.3 CONTROLLING OF THE HUMAN SCLERA OPTICAL PROPERTIES

The control of tissue optical properties is very important for many applications.<sup>3,84-92</sup> The selective optical clearing of tissue layers should be very useful for the functional tomography of the human organs, in particular, the eye globe, and for tissue scattering spectroscopy. For instance, transscleral laser technologies are based on the tissue optical clearing effect.<sup>87</sup> The coherence-domain methods, especially optical speckle correlometry, are very useful for monitoring changes in optical and structural parameters of the human sclera in a process of tissue clearing.<sup>3,84,85</sup> One of the fruitful ways for human sclera optical property control is its impregnation by a osmotically active chemical that leads to matching of refractive indices of collagenous fibrils ( $n_C$ ) and interstitial fluid ( $n_I$ ).<sup>84,85</sup> Optical techniques for noninvasive monitoring of *glucose* concentration in living tissues use the same effect of tissue scattering control.<sup>88,89,92</sup> In the time-dependent process of the tissue components refractive indices matching  $m = n_C / n_I \rightarrow 1$ , and the ratio of the scattering coefficients for different degree of matching is expressed as<sup>84,85</sup>

$$\mu_s(t) \cong \mu_s(0) \{ [m(t) - 1] / [m(0) - 1] \}^2. \quad (10)$$

For a high degree of matching which is easily attainable in experiments with human and mammalian sclera,  $m(t) \cong 1.001$ , as well as for unmatched scleral tissue  $m(0) \cong 1.1$ . Therefore, the scattering coefficient dramatically decreases,  $\mu_s(t) \cong 10^{-4} \mu_s(0)$ , and tissue response should transfer from a multiple scattering mode to a single or low-step scattering one for which coherent-domain effects should dominate.

Our experimental study of the human sclera optical clearing was performed *in vitro* for cut samples of about  $1 \times 1 \text{ cm}^2$  in area and 0.4–0.8 mm in thickness obtained from eight autopsy eyes, from ages 61 to 72 years. Three types of water-soluble chemical agents were applied: *trazograph* (derivative of 2-4-6 triiodobenzene acid, molecular weight about 500), *glucose* (~180), and *polyethylene glycol* (PEG) (~6000 and ~20 000).

Visually the characteristic changes of the far-zone speckle structure were observed on the screen in the far diffraction zone using a charge coupled device (CCD) camera.<sup>85</sup> After the osmolyte administration first, there were no visually observed speckles. In a few minutes (1–3 min, depending on the sclera thickness, its initial transmittance, type and concentration of osmolyte) an isotropic speckle pattern consisting of small-sized speckles appeared. For longer periods the speckle pattern became inhomogeneous with the large-sized speckles in the central part; finally, the main part of the transmitted light was concentrated around the incident beam axis (see Figure 8).

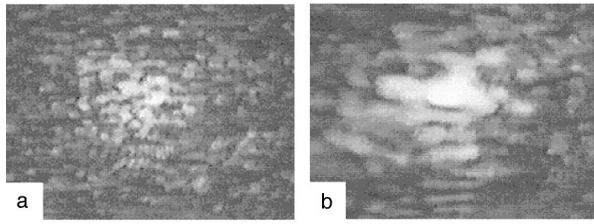


**Fig. 8** CCD images of the far-zone speckle patterns for early ( $\sim 2.5$  min) (a) and later ( $\sim 10$  min) (b) stages of the sclera optical clearing using *trazograph* (60%) administration.

The time evolution of the normalized intensity autocorrelation function  $\tilde{g}_2(\tau)$  [see Eq. (7)] measured for the human sclera sample using a speckle correlometer (see Figure 3) can be seen in Figure 9. The evolution of the form of the main correlation peak is caused by the transition between two scattering modes: for short intervals (1–2 min)  $\tilde{g}_2(\tau)$  is rather “exponential” and for longer intervals is closer to the Gaussian one. For the initial stages of process “multiscality” of intensity fluctuations is characteristic (at least three different slopes of the  $\tilde{g}_2(\tau)$  function measured at 120 s after *trazograph* administration are observed). At the final stages of optical clearing the half-width of the autocorrelation peak asymptotically rises to a value of about  $(0.3\text{--}0.4) \times 10^{-3}$  s which is closely correlated with  $\Delta\tau = w/v$ , defined by the illuminating beam waist radius  $w$  and the speed of scanning  $v$ . That can be used as the criterion of the completion from multiple to single scattering transition. The evolution of the peak form caused by time-dependent variations of tissue structure is illustrated by the typical temporal dependence of the exponential factor  $\nu_I$  [see Eqs. (4) and (5)]. It should be stressed that the averaged intensity transmittance  $\langle I_s \rangle / I_0$  and parameter  $\nu_I(t)$  have quite different rates of increase:  $\nu_I$  is very sensitive to the osmolyte on the earlier stages of tissue clearing ( $\sim 1.5$  min) and maximal tissue transmittance happened at  $\sim 10$  min. A possible explanation of such a discrepancy lies in the different responses of these characteristics to the transition

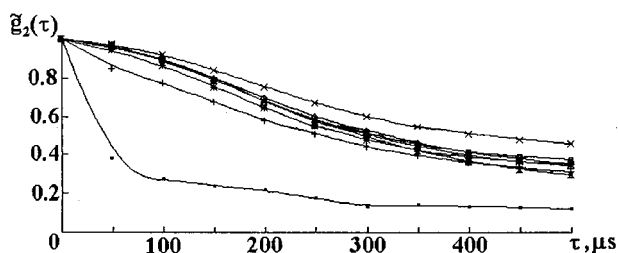


**Fig. 9** Intensity autocorrelation functions measured in the far zone using the scanning spatial speckle correlometer (Figure 3). The human sclera sample thickness is equal to 0.55 mm. Measurements were done for different time intervals of tissue impregnation by *trazograph* solution (60%): ■ 120 s; + 220 s; \* 320 s; □ 420 s; × 520 s; ◇ 620 s; △ 720 s; ⋈ 820 s.

from multiple to single scattering caused by refractive index matching of tissue components. The exponential factor  $\nu_I$  should be sensitive to the transition from homogeneous speckles to inhomogeneous ones (corresponding to the earlier stage of clearing) and maximal averaged intensity transmittance should be expected only for totally immersed scatterers which take place in a long period of tissue impregnation by an osmolyte.

Monte Carlo modeling of the initially collimated photon transport within the sclera tissue represented as a fibrous structure comprised of thin and long collagenous cylinders randomly distributed within the ground medium allows us to understand the character of transition from multiple to single scattering due to refractive index matching.<sup>85</sup> Results of such modeling for a system of scattering cylinders with a mean diameter of about 100 nm and refractive index  $n_C = 1.474$  surrounded by the interstitial medium with a changeable refractive index show that already for partly matched refractive indices the unscattered and singly scattered photons dominate. The validity of such calculations was checked using spectral measurements of the human sclera for different stages of its clearing.<sup>85</sup>

Another peculiarity clearly observed especially at final stages of the process is the presence of the low-amplitude quasiperiodic oscillations of the averaged transmitted intensity, the exponential factor  $\nu_I$ , and the half-width of the correlation peak with the characteristic time scale of about 1.5–2.0 min (see Figures 9 and 10). Such quasiperiodic oscillations can be induced by the temporal-spatial irregularity of osmolyte diffusion within the tissue volume. The oscillating character of tissue response can be explained as a multistep origin of fluid diffusion. The first step osmolyte penetration into tissue leads to refractive index matching of interstitial fluid and hydrated fibril collagen—the significant translucence of tissue growth. The second step is characterized by the interaction of osmolytes, contained within the renovated interstitial liquid, with fibril collagen which leads to collagen dehydration and consequent growth of its refractive index that slightly breaks down optical matching and causes a slight decrease of transmittance. Subsequent disbalance of water-osmolyte concentrations leads in turn to penetration of an additional amount of osmolyte into the sample which causes reestablishment of the refractive index matching condition and a corresponding light transmittance—this is the origin of the third step. Such weak oscillations exist during the total process of chemical administration (up to 40–60 min).

The normalized averaged intensity  $\langle I_s \rangle / I_0$  presented in Figure 10 shows the dynamics of tissue clearing. Such dependence can be used for estimation of diffusion coefficients of the interacting fluids: *trazograph* and water, *glucose* and water, etc. Basing on the theoretical background given in Ref. 85 we can estimate the coefficient of diffusion for

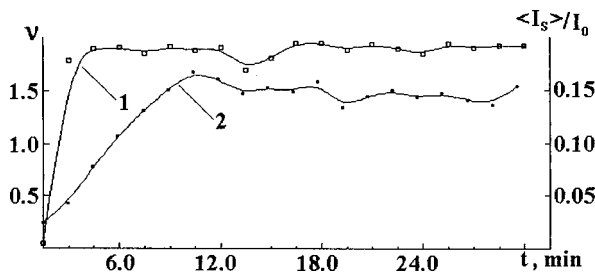


**Fig. 10** Typical temporal functions of the exponential factor  $\nu_1$  (1) and the normalized averaged intensity  $\langle I_s \rangle / I_0$  (2) measured at the observation point for the human scleral sample impregnated with *trazograph* solution (60%),  $\lambda = 633$  nm.

*trazograph* supposing that water and *trazograph* have the same paths for diffusion. The experimental data presented in Figure 10 allow us to estimate  $D_T$  values for  $n_C = 1.474$ ,  $n_W = 1.332$  (water),  $n_I(0) = 1.345$ , and  $\mu_a = 0.2 \text{ mm}^{-1}$  (see Table 2). It is easily seen that estimated values of  $D_T$  for the certain scleral sample have quite reasonable rms errors as well as mean values of  $D_T$  that differ from sample to sample. On the average, experimental values of diffusion coefficients for *glucose* and *trazograph* are not far from ones for diffusion of low weight molecules in water.<sup>93</sup> As for water diffusion induced by *polyethylene glycol* activity, again values of the diffusion coefficient are very close to diffusion of water in water.<sup>94</sup>

It is expected that the change of the optical properties of tissue, caused by the transition from multiple to single scattering, should be accompanied by a change in the state of polarization of the scattered light. That can be described using the first- and second-order statistical characteristics [see Eqs. (8) and (9)].<sup>84,85,95</sup> At the early stages of the tissue clearing both polarization states of the scattered light ( $\langle I_{\parallel} \rangle$  and  $\langle I_{\perp} \rangle$ ) give approximately equal contributions to the mean speckle intensity  $\langle I_s \rangle$ . The decrease of the sclera turbidity is accompanied by the increase of the speckle sizes appearing of the specu-

**Table 2** Mean values and rms of diffusion coefficient for *trazograph*  $D_T$  in the human sclera samples determined on the basis of experimental data for the averaged intensity transmittance at  $\lambda = 633$  nm.

Sample No.	Thickness of sample, mm	Coefficient of diffusion, $\text{cm}^2/\text{s}$	rms of diffusion coefficient, $\text{cm}^2/\text{s}$
1	0.5	$1.46 \times 10^{-5}$	$1.90 \times 10^{-6}$
2	0.5	$4.00 \times 10^{-6}$	$1.15 \times 10^{-6}$
3	0.4	$5.29 \times 10^{-6}$	$7.58 \times 10^{-7}$
4	0.4	$1.20 \times 10^{-5}$	$1.01 \times 10^{-6}$

lar component. Therefore, the state of polarization of the transmitted light is predominantly identical to one for the unscattered beam. Experimental data, presented in Figure 11, nicely illustrate that. Moreover, they demonstrate that for living tissue a multiple-single scattering transition (i.e., optical translucence, improvement of polarization) is reversible when the osmolyte bath is replaced by a physiological solution and vice versa when the osmolyte is administered again. Besides, as follows from Figure 11, the polarization measurements are quite sensitive to changes of the tissue structure caused by sufficiently long interaction of tissue with *trazograph*. Our corresponding histological observations for sclera samples kept in *trazograph* (60%) solution during 30 min showed rather minor changes of tissue structure which are characterized by a moderate tissue swelling.

It must be noted that transparent sclera samples have a "domain" structure with quite different scattering (polarization) properties for the individual areas of about  $0.1\text{--}1 \text{ mm}^2$ . Such a domain structure caused by the spatial nonuniformities of the *trazograph* diffusion is clearly manifested in the time series of the speckle intensity fluctuations for two different polarization states of the scattered field as well as in cross-correlation function  $r_{\perp\parallel}(\tau)$

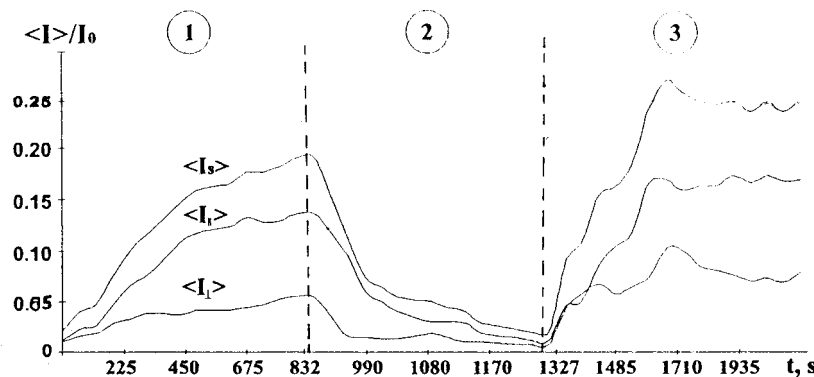


**Fig. 11** The time-dependent mean speckle intensity  $\langle I_s \rangle$  averaged over the scanning trace (1.5 mm) and its polarization components  $\langle I_{\parallel} \rangle$  and  $\langle I_{\perp} \rangle$  measured in the paraxial region for the human sclera sample of thickness 0.4 mm: 1, 2, and 3—the subsequent measurements for sample kept at first in 60% solution of *trazograph* (1), then in physiological solution (0.9% NaCl) (2), and finally again in *trazograph* (60%) solution (3);  $\lambda = 633$  nm.

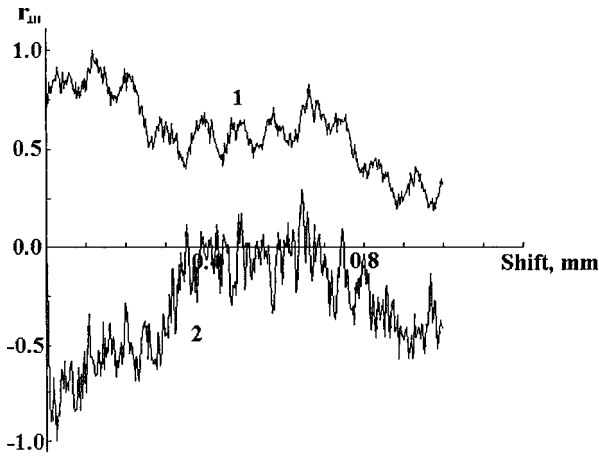


**Fig. 12** Evolution of the cross-correlation function of the speckle intensity fluctuations with two orthogonal states of linear polarization ( $r_{||}$ ) caused by the decrease of human sclera turbidity due to *trazograph* (60%) administration: 1—200 s of tissue sample kept in *trazograph* solution; 2—400 s.

behavior (see Figure 12). The mean area of such domains goes down with the time of osmolyte administration. For *trazograph* it changes from about 1 mm<sup>2</sup> (for  $t \approx 3.3$  min) up to 0.12 mm<sup>2</sup> (for  $t \approx 6.6$  min). The polarization properties of domains change correspondingly.

### 3 FOCUSED LASER BEAM DIFFRACTION AS A TOOL FOR BLOOD AND LYMPH FLOW MONITORING IN MICROVESSELS

#### 3.1 THE PECULIARITIES OF THE FOCUSED GAUSSIAN BEAM DIFFRACTION

Let us consider scalar diffraction of the focused Gaussian beam (FGB) which is moved along the corrugated random phase screen<sup>76,96-99</sup> (see Figure 13). The screen profile function, which models the statistical properties of the flow, is assumed to be determined by a stationary Gaussian stochastic process with zero mean value, the profile variance  $\Sigma^2$ , and the correlation length  $L_C$ . For the far-field dif-

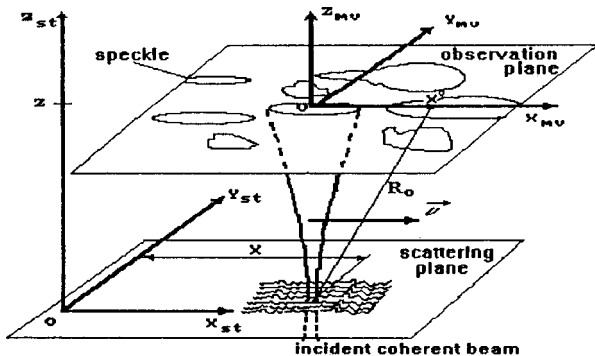


**Fig. 13** Focused Gaussian beam diffraction at the moving random phase screen.

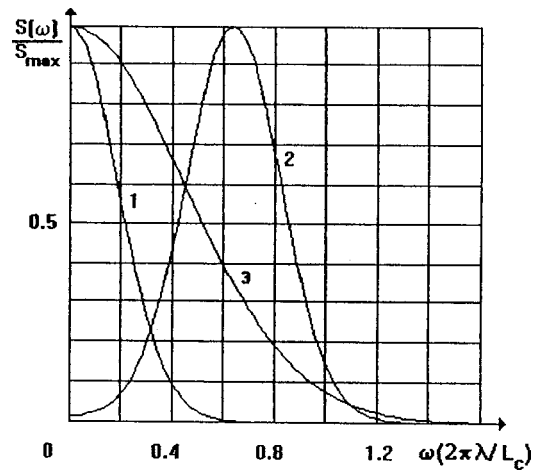


**Fig. 14** The normalized theoretical spectra of dynamic speckle intensity fluctuations for the beam waist radius  $w_0 = 10\lambda$ : 1— $\sigma = 0.01\lambda$ ,  $X^0 = 0$ ; 2— $\sigma = 0.01\lambda$ ,  $X^0 = 2Z$ ; 3— $\sigma = 0.3\lambda$ ,  $X^0 = 2Z$ .

fraction of FGB the power spectrum of intensity fluctuations can be represented as the homodyne (I) and heterodyne (II) terms<sup>96</sup>

$$S(\omega) = \left[ C_1 \left( \frac{2\pi}{\beta} \right)^{0.5} \exp\left( -\frac{\omega^2}{8\beta} \right) \right]_I + \left( C_2 \left( \frac{\pi}{\beta} \right)^{0.5} \left\{ \exp\left[ -\frac{(\omega - \omega_0)^2}{4\beta} \right] + \exp\left[ -\frac{(\omega + \omega_0)^2}{4\beta} \right] \right\} \right) \right]_{II}, \quad (11)$$

where

$$\beta = \frac{M}{L_C^2 + 2MW_0^2}, \quad \omega_0 = \frac{4\pi M \left( \frac{W_0}{L_C} \right)^2 \frac{X^0}{Z}}{1 + 2M \left( \frac{W_0}{L_C} \right)^2},$$

where  $W_0$  is the beam waist radius,  $X^0$  is the fixed speckle observation point coordinate in the mobile coordinate system ( $X_{mv}$ ,  $Y_{mv}$ ,  $Z_{mv}$ ), and  $Z$  is the distance between the scattering and observation planes.  $M$ ,  $C_1$ , and  $C_2$  are parameters dependent on  $\Sigma^2$  and  $L_C$ .<sup>96</sup> All the length dimensions are normalized to the light wavelength  $\lambda$ .

For a weakly scattering phase screen (model of a thin vessel),  $M = 1$ ,  $C_1 \ll C_2$ , and for a deep phase screen (model of a thick vessel),  $M \sim \Sigma^2$ ,  $C_1 \gg C_2$ . For thin vessels, the appearance of a high-frequency peak in the spectrum of intensity fluctuations ( $\omega = \omega_0$ , heterodyne part of spectrum) due to interferential interaction of the specular and scattered components is expected. The specular component (transmitted or reflected) serves as a reference wave. The value of  $\omega_0$  depends on the observation angle of the speckles ( $X^0/Z$ ) (compare curves 1 and 2 in Figure 14). For a weakly scattering screen

due to small rms values of profile fluctuations ( $\sigma = \lambda \Sigma$ ) the power spectrum  $S(\omega)$  for  $X^0 \neq 0$  contains only a high-frequency component. For a deep phase screen due to suppression of the specular component its interferential interaction with the scattered light disappears, and  $S(\omega)$  contains only a low frequency component even for large observation angles (see curve 3 in Figure 14). As follows from theory and experimental study the statistical properties of the transmitted (or reflected) light essentially depend on the observation angle (see Figures 14 and 15). Such speckle statistics with a small number of scatterers can be classified as non-Gaussian statistically inhomogeneous.

The unscaled value of  $X = vt/\lambda$  is used as the variation describing the displacement of the waist center of a focused beam ( $v$  is the motion velocity of a phase screen relative to a beam;  $t$  is the time). The scaled frequency  $\nu = (\omega/2\pi)(v/\lambda)$ . Similar to the conventional Doppler method, the frequency shift value is a linear function both of scatterer velocity and speckle observation angle only for an essential number of scatterers. For a small number of scatterers,  $N < 5$ , the additional strong dependence of the frequency shift on  $N$  is expected.<sup>96,99</sup>

### 3.2 EXPERIMENTAL SETUP AND MEASURING TECHNIQUE

The optical scheme of setup used for the experimental investigations of blood and lymph flow in microvessels contains a He-Ne laser ( $\lambda = 633$  nm) with a focused beam (Figure 16).<sup>97,98</sup> Blood or lymph flow modulates the strongly focused laser beam in the waist plane. This leads to the speckle dynamics in Fraunhofer zone of diffraction. Scattered intensity is detected in the asymptotic region. Averaging over the 128 momentary spectra of the speckle intensity fluctuations was performed. The

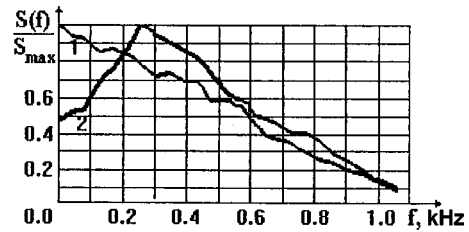


**Fig. 15** The normalized experimental spectra of dynamic speckles intensity fluctuations for two observation angles: scattering from random flow  $X^0 = 0$  (1),  $X^0 = 3W/2\pi$  (2),  $w_0 \approx 2.3\lambda$ , averaged spectra for 256 particular momentary spectra.

setup provides three-dimensional (3D) spatially resolved measurements for an individual superficial microvessel of rat mesentery at a depth of up to 200–300  $\mu\text{m}$  with a spatial resolution of about 3–5  $\mu\text{m}$ . An optical microscope supplied by the TV camera allows one to observe the blood or lymph flow in a microvessel visually.

Using the method of FGB diffraction the following parameters characterizing blood or lymph flow velocity distribution were defined. The mean value of flow velocity is

$$V = \Delta F / D,$$

where  $\Delta F$  is the averaged spectrum bandwidth,  $D$  is the diameter of a microvessel studied. The parameter indicating the deviation of spectrum shape from a Gaussian curve is

$$\Sigma_V = \left( \int_0^{\Delta F} [S(f) - G(f)]^4 df \right) / \left( \frac{1}{\Delta F} \left[ \int_0^{\Delta F} [S(f) - G(f)]^2 df \right]^2 \right),$$

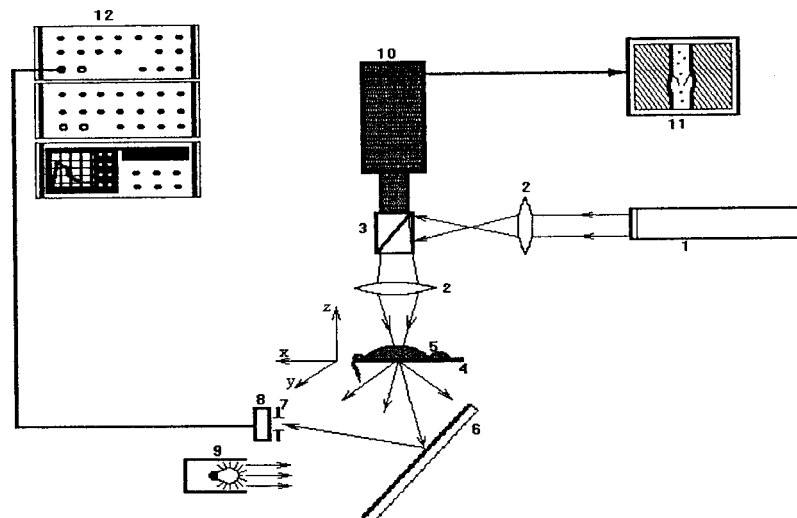


**Fig. 16** Time-resolved speckle microscope for blood and lymph flow measurements in microvessels. 1—He-Ne laser; 2—micro-objective; 3—beam splitter; 4—stage; 5—rat; 6—mirror; 7—diaphragm; 8—photomultiplier tube (PMT); 9—lamp; 10—TV camera; 11—monitor; 12—spectrum analyzer 0–2 kHz.

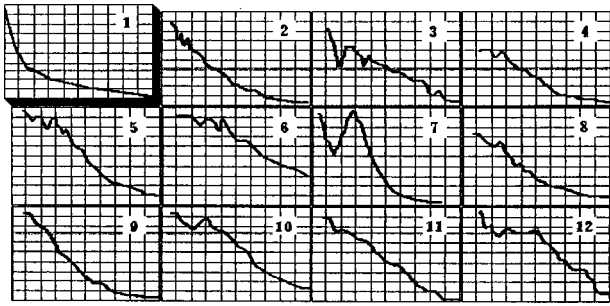


**Fig. 17** Typical normalized averaged spectra of the scattered intensity fluctuations  $S(F)/S_{\max}$  at FGB diffraction measured for: 1—blood microvessel with  $D=12\ \mu\text{m}$ ; 2–12—for various lymph microvessels of different rats. Frequency range is 30–1500 Hz.

where  $S(f)$  is the averaged experimental intensity fluctuation power spectrum of speckles and  $G(f)$  is the Gaussian spectrum having the same values both of spectrum bandwidth and power. Parameter  $\Sigma_V$  demonstrates the velocity range presenting in the flow and, besides that, gives information about spatial-temporal velocity changes within the measuring volume.

### 3.3 MEASUREMENTS OF FLOW PARAMETERS OF BLOOD AND LYMPH IN MICROVESSELS

Experiments were performed on white rats narcotized by intramuscular injection of Nembutal. Mesentery obtained through an incision in the anterior abdominal wall was placed on thermostabilizing microscope stage ( $38\ ^\circ\text{C}$ ).<sup>97,98</sup> The state of lymph microvessels (60–150  $\mu\text{m}$  in diameter) not having spontaneous phase contractile activity was analyzed. The narrow blood microvessels were investigated as well. Alterations in diameter of vessels, rate, and amplitude of induced phase contractions were registered with the help of a TV microscope.

*Staphylococcal* toxin (ST) was administered to the mesentery as an active lymphotropic agent. The results of theoretical investigation of FGB diffraction in capillaries show that the speckle intensity fluctuations bandwidth  $\Delta F$  is proportional to velocity of flow analyzed and  $\Delta F$  essentially depends on scattering properties of the flow.<sup>96,99</sup> The last causes some difficulties in direct measurements of an absolute value of blood or lymph flow velocity. The strong dependence of  $\Delta F$  value on the diameter  $D$  of investigated blood microvessels was observed in the experiments. The typical average spectra obtained at FGB scattering either from a narrow blood microvessel ( $D=12\ \mu\text{m}$ ) and from a number of different lymph microvessels with the average diameter  $D=119\pm 7\ \mu\text{m}$  are shown in Figure 17. As was expected, the blood flow spectrum has decreasing character but despite theoretical predictions, the shape of the spectrum differs greatly from Gaussian function. Similar spectra have been studied thoroughly in earlier modal experiments (see, for example, Refs. 16 and 100).

Essential differences between the spectra obtained from lymph and blood flows appeared. The spectra of lymph flow have a considerably complicated shape; in some cases the spectra observed have two or more peaks. The spectra presented in Refs. 96–98 demonstrate the essential difference of the lymph flow parameters for the vessel center and for the regions in the vicinity of its edges. Sometimes the lymph flow had a shuttle-stream mode or assisted only at the central part of vessel. Evidently, such types of flow are reflected in the variety of spectra presented in Figure 17. It has been shown that the FGB scattering technique can be successfully used for monitoring the lymphotropic drug effect on living organisms.<sup>96–98</sup>

So, the speckle-interferential method using diffraction of the focused laser beam may be efficiently applied for measuring of relative changes of blood and lymph flow parameters in native microvessels. For extremely narrow microvessels, both speckle-interferential and Doppler methods do not allow one to measure directly the absolute value of flow velocity; they need the preliminary calibration.

## 4 SPECKLE AND SPECKLE-INTERFEROMETRIC TECHNIQUES FOR DETECTION OF BIOVIBRATIONS

### 4.1 INTRODUCTION

At present a number of optical techniques for biovibration monitoring are developed. For example, a fiber-optical sensor was successfully applied for monitoring the heartbeats of the patients during their MRI tomographical observation.<sup>101</sup> Noncontact laser biovibration measuring techniques are described in detail in Khanna's works,<sup>34,102</sup> where vibrations of the basilar membrane of the inner ear are investigated by the laser interferometric heterodyne method. To analyze vibrations of the tympanic membrane Stasche et al. used laser-Doppler vibrometry.<sup>35</sup> Holographic vibration analysis of the tympanic membrane has also been reported.<sup>103</sup> Optical remote sensing of the heartbeats is discussed by Dacosta.<sup>104</sup> The fact that coherent radiation scattered by bio-objects is accompanied by the formation of speckle fields was not completely taken into account for biovibration measurements. The interference between the speckle-modulated and reference fields has a number of features that require a thorough study. The development of speckle techniques for biovibrations measurements is directly connected with the theoretical description of coherent light diffraction in nonstationary, random heterogeneous media.<sup>105–107</sup> At present several speckle techniques for biovibration detection are available.<sup>105–111</sup> A diagnostic probe, described in Ref. 108, includes the miniaturized electronic speckle pattern interferometry system and the fiber optic elements coupled with a matrix detector. Subsequent frame-by-frame processing produces a

high quality 3D spatial representation of the vibrational pattern. The diagnostic probe is being developed for a quantitative vibration analysis of the tympanic membrane and vocal cord. The possibility of cardiovascular measurements using speckle and speckle-interferential methods are analyzed in Refs. 105–107 and shortly overviewed in this article. The FGB speckle technique was successfully applied for pulse wave and throat vibration monitoring.<sup>107</sup>

#### 4.2 HOMODYNE SPECKLE INTERFEROMETRY

The homodyne speckle interferometer on the base of the Michelson interferometer with diffuse reflecting plates instead of mirrors for both arms under the coherent light excitation has the random amplitude-phase spatial modulation of the output signal.<sup>106</sup> Supposing that fields in both arms have identical linear polarization and object (one of the scattering plates) vibrations have harmonic law, then the total field intensity at the point  $\xi(\xi, \eta)$  of the observation plane can be described as<sup>106</sup>

$$I(\xi, t) = I_1(\xi) + I_2(\xi) + 2[I_1(\xi)I_2(\xi)]^{0.5} \cos\{\Delta\Phi(\xi, t) + \Delta\Psi(\xi) + 4\pi(\Delta z_0 + l_0 \sin \Omega t) / \lambda\}, \quad (12)$$

where  $\Delta\Phi(\xi, t) = \Phi_2(\xi, t) - \Phi_1(\xi)$ ;  $I_1(\xi)$ ,  $I_2(\xi)$ ,  $\Phi_1(\xi, t)$ , and  $\Phi_2(\xi)$  are the random intensity and phase distributions of the reference (1) and the object (2) speckle fields;  $\Delta\Psi(\xi) = \Psi_2(\xi) - \Psi_1(\xi)$  is the deterministic phase difference of interfering waves;  $2\Delta z_0$  is the stationary difference of wave optical paths in the interferometer;  $l_0$  and  $\Omega$  are the corresponding amplitude and frequency of vibrations.

For *unmatched speckle fields* [ $\Delta\Psi(\xi)$  varies more than  $\pi$  radians and  $\Delta\Phi(\xi) = \text{const}$  over the spatial extent of a speckle] the speckle pattern in the observation plane should be modulated by regular interferential fringes. Fringe spatial configurations and their period are determined by deterministic phase difference  $\Delta\Psi(\xi)$ . The fringe orientation is perpendicular to the grad [ $\Delta\Psi(\xi)$ ] with the period  $\Lambda(\xi) = 2\pi / |\text{grad}[\Delta\Psi(\xi)]|$ , and they undergo shifting and bending by a random value while moving from one speckle to another. If the object vibrates, then the fringes are displaced by  $M$  periods ( $2l_0 = M\lambda/2$ ) synchronously and by the same value within the different speckles. Detection of the fringe shift within a distinct speckle allows one to measure  $l_0$  and  $\Omega$  of the object vibrations. It follows from Eq. (12) that in different speckles fringes are shifted.

Adjusting the interferometer [by  $\Delta\Psi(\xi)$  changing] we can make the fringe period  $\Lambda$  appreciably larger than the lateral speckle dimensions. That leads to an increase of the output signal amplitude due to the possible use of a large photodetector aperture equal to a distinct speckle size. In the limit when  $\Delta\Psi(\xi) = \text{const}$  over the whole observation plane, the interfering speckle fields will be *matched*. To attain the matching condition for focused illuminat-

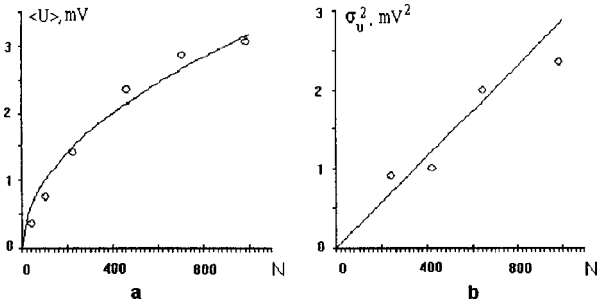


**Fig. 18** Experimental and theoretical plots of the speckle-interferometer output signal averaged amplitude  $\langle U \rangle$  (a) and its variance  $\sigma_u^2$  (b) on the number of speckles fall within the receiving aperture (large vibration amplitudes,  $l_0 \sim \lambda$ , unchangeable speckle size, about 300 realizations of the reference speckle field).

ing beams it is sufficient to equalize path lengths of the interferometer. Because the speckle-field matching leads to an increase of the output signal of the vibrometer, we will consider the statistical properties of such a regime in more details.

A speckle vibrometer can work in two measuring modes: with a high amplitude of vibrations ( $l_0 > \lambda/4$ ), the so-called “fringe counting” mode, and with a small amplitude of vibrations ( $l_0 < \lambda/4$ ), when the random amplitude of the output signal additionally depends on initial phase.

If  $N$  speckles arrive at the receiving aperture, then for  $N > 4$  the first-order statistics of the output signal will be Gaussian, i.e., the complex amplitude of this signal undergoes Rayleigh distribution.<sup>106</sup> Experimental data well demonstrate such statistics of the speckle-interferometer output signal for large amplitude of vibrations,  $l_0 \sim \lambda$ .<sup>106</sup> In addition, the corresponding experimental function for averaged amplitude  $\langle U \rangle$  and its variance  $\sigma_u^2$  on the number of speckles that fall within receiving aperture show the way for increasing the signal-to-noise ratio in homodyne speckle interferometers (see Figure 18). Such functions are well described in the framework of the theoretical predictions of Ref. 109:

$$\langle U \rangle \cong \delta^2(N)^{0.5}, \quad \sigma_u^2 \sim N, \quad (13)$$

where  $\delta$  is the average lateral speckle size, for the round aperture with the diameter  $2R$ ,  $N = (2R/\delta)^2$ ; we suppose that interfering field intensity does not change when speckle size changes.

So, to increase the output signal amplitude it is important to arrange the optical scheme of the speckle interferometer which provides a great number of received speckles with maximal average size. As it follows from above that we should use focused beams in both arms of the interferometer and a large enough receiving aperture.

When the amplitude of normal surface vibration of the object is not small, as a rule, the angular and lateral vibrations appear. This leads to periodic lateral shifts of the subject speckle field, which cause additional amplitude-phase modulation at every

point at the output plane and corresponding low-frequency amplitude modulation of the interferometer output signal.<sup>106</sup> The depth of this modulation depends on the particular realization of the reference and subject speckle fields and changes in the range 0%–100%. It was found that the main contribution to the amplitude modulation is made by a number of closely packed speckles playing the dominating role in signal formation. Dimensions of this region and its position depend on particular interfering speckle-field realization. The blocking of this area by using an opaque screen at the receiving aperture leads to suppression of additional modulation.<sup>106</sup>

For small amplitudes of vibration ( $l_0 < \lambda/4$ ) statistics of the output signal of the interferometer is quite different. As follows from experimental and theoretical data, the distribution of amplitude modulus of the signal,  $|U|$ , is exponential:<sup>106</sup>

$$p(|U|) = 2(\pi N \sigma_n^2)^{-0.5} \exp(-U^2/2N\sigma_n^2), \quad (14)$$

with the most probable value equal to zero. Here  $\sigma_n$  is the variance of the random value which depends on the surface structure and parameters of the interferometer. The averaged value and variance have the same dependence on  $N$  as for a large amplitude of vibrations [see Eq. (13)]:

$$\langle |U| \rangle = (2N\sigma_n^2/\pi)^{0.5}, \quad \sigma_{|U|}^2 \cong 0.36N\sigma_n^2. \quad (15)$$

In accordance with the above consideration the output signal of the homodyne speckle interferometer can be presented as

$$U_i(t) = A_i \sin[\phi_i + AL \cdot H(t)], \quad (16)$$

where  $H(t)$  is the normalized signal (which variance equals to unity) that describes the form of bio-object surface oscillations,  $A_i$  and  $\phi_i$  are random values, determined by conditions of speckle-interferogram detection and the rough surface realization (with number  $i$ ), and  $AL$  is the vibration amplitude. This relation is also valid for the differential interferometer for which  $AL$  denotes the vibration amplitude difference of surface oscillations in two points of light illumination.

Using the differential speckle interferometer, the human pulse wave monitoring was carried out. Pulse waves were observed at the points of wrist skin surface (in Tibetan pulse diagnostics these points are called "tson," "khan," and "chug").<sup>106</sup> The optical signal was registered at the point where speckle fields were matched. In this region the interferometer output signal is maximal. Received pulsegrams are in close agreement with the data of Ref. 101.

The pulse wave investigations, based on analysis of space-time projection of the differential speckle-interferometer output signal, should be promising for cardiodynamics, but it is expedient to elimi-

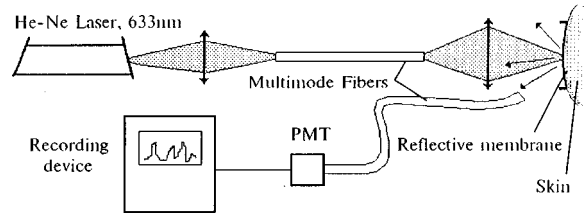


Fig. 19 Scheme of the sensor for the pulse wave monitoring.

nate the influence of the lateral shifts of the skin surface by the appropriate signal filtration.<sup>107,110</sup>

### 4.3 ANALYSIS OF SKIN VIBRATION USING FGB DIFFRACTION

The simplest optical vibrometer for medical applications can be built using FGB diffraction (see Figure 19).<sup>107</sup> But such simplicity of the optical design should be paid by nontrivial description of the response function of the vibrometer. For FGB diffraction the scattered field intensity fluctuations are related to the object vibrations via a nonlinear random function. Regular changes of the speckle field (speckle displacements and their decorrelation) due to oscillations of the scattering surface form a signal at the photodetector that contains spectral components of the surface vibrations. The complex movement of the reflecting surface leads to additional nonlinearities of the response function. For example, the periodic human skin surface motion caused by pulse waves can be presented as a combination of at least three components: normal, angular, and lateral. For the measuring system used (see Figure 19), normal oscillations do not affect the output signal; small angular vibrations are responsible for lateral speckles oscillations in the observation plane (without speckle decorrelation) and small lateral surface shifts cause a partial decorrelation of speckles, so if the surface oscillates by a periodical law, the scattered field temporal intensity fluctuations  $I(t)$  also have a periodic component. A nonlinear function  $I(t) = F[X_{\tau\nu}(t)]$  connects these fluctuations  $I(t)$  and the scatterer vibration law  $X_{\tau\nu}(t)$ , where  $F$  is a nonlinear random operator which depends on the size of the illuminated area, conditions of speckle observation, and on the particular realization of the random surface (rough skin surface).

The nonlinear distortion (NL) of the registered signal and the degree of random deviation (RND) of the measured value from the average can be estimated using the following definition:<sup>107</sup>

$$NL = \sum_n \langle I_n^2 \rangle / \langle I_1^2 \rangle, \quad RND = \sigma_1 / \langle I_1 \rangle,$$

where  $I_n$  is the amplitude of the  $n$ th harmonic of intensity fluctuation spectrum,  $\sigma_1$  is the first har-

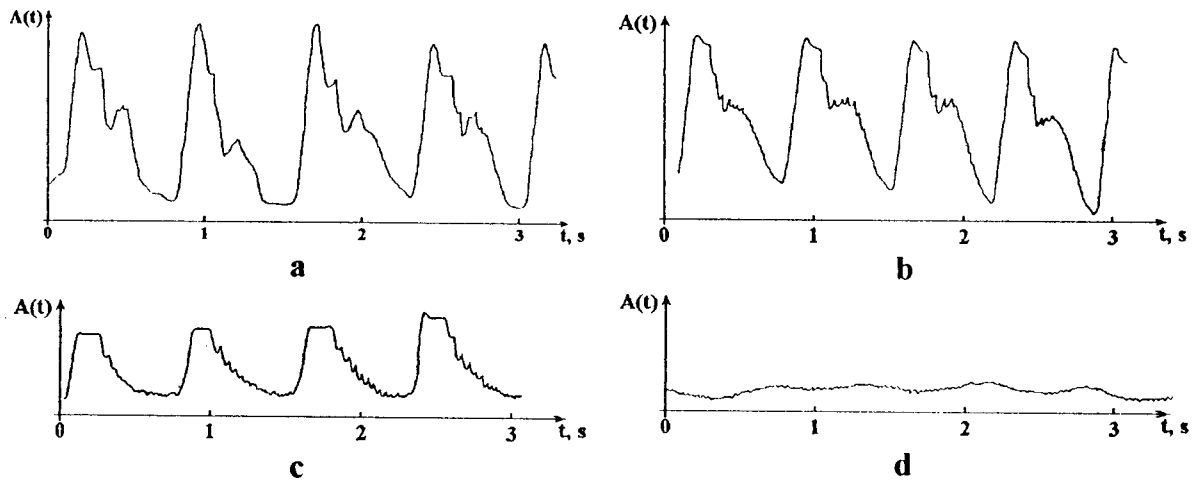


**Fig. 20** Experimental pulsegrams, radial pulse of healthy young man (24 years old) registered for different values of external pressure  $P$  applied to the arm: (a)  $P=0$ ; (b)  $P=60$ ; (c)  $P=90$ ; (d)  $P=110$  mm Hg.

monic standard deviation,  $\langle \dots \rangle$  indicates ensemble averaging, and  $n$  changes from 2 to infinity.

Computer modeling of statistical properties of intensity fluctuations of FGB scattered from the vibrating rough surface was done using Kirchhoff approximation for the scattered field complex amplitude and Gaussian statistics of a rough surface.<sup>107</sup> It was shown that for lateral and angular vibrations of the surface statistical and nonlinear effects do not seriously distort the output signal. That allows one to determine the surface vibration law with a high precision if lateral vibration amplitude  $a_0 < l_c$  and amplitude of angular vibration  $\delta\alpha \leq 1^\circ$ .

The scheme of the handy optical device designed is given in Figure 19. This sensor transforms the skin vibrations caused by pulse waves into regular speckle motion that is detected. Using a thin rubber membrane attached to the skin surface allows one to avoid tissue volume scattering and provide more standardized reflecting properties. The radial pulse wave monitoring has been carried out for a healthy 24-year-old male for different values of external pressure applied to the biceps area (see Figure 20). It should be noted that the sensor is a good prototype for a portable computer aided pulse wave sensor assembled on the base of a laser and photodiodes with multimode fiber pigtailed.

## 5 SPATIAL DOMAIN LASER TECHNIQUES FOR TISSUE TESTING

### 5.1 PROPAGATION OF A SPATIALLY MODULATED LASER BEAM THROUGH A RANDOM PHASE OBJECT

Laser beams, spatially modulated by a regular interference pattern, are widely used for surface profile,<sup>112</sup> form,<sup>113</sup> and displacement measurements,<sup>113,114</sup> as well as for cell counting and biofluids flow diagnostics.<sup>28,115</sup> These methods usually employ a small spacing of interference fringes com-

parable to the sizes of object inhomogeneities. The fringe spacing in the illuminating beam considerably exceeding object inhomogeneity sizes leads to new correlation effects in the scattered field and, therefore, to new measuring speckle technologies for inspection of random phase objects.<sup>116-119</sup> The interference fringes of average intensity with contrast varying along the longitudinal axis  $z$  are formed in the scattered speckle-modulated field. If the beam aperture size and fringe spacing are rather large, the fringes modulate the field speckle structure and fringe contrast evolution along axis  $z$  is determined by statistical parameters of the object and fringe spacing.

In experiments the fringes in the illuminating beam were provided by a spatial-temporal optical modulator; the fringes of average intensity in the scattered field were recorded by the photodetector with a slit aperture, oriented along the fringes (the slit aperture served for averaging of the scattered field speckle modulation). As a result the modulation depth of the output signal was equal to the relative fringe contrast<sup>119</sup>

$$V(z)/V_0 = |\mu(z)|, \quad (17)$$

where  $V(z)$  is the average intensity contrast,  $V_0$  is the initial contrast of laser incident beam, and  $|\mu(z)|$  is the modulus of the transverse correlation coefficient of the complex scattered field amplitude.

For experimental modeling of biological tissues and cell structures with various statistics of phase inhomogeneities, special plane phantom specklegrams were designed.<sup>119</sup> Figure 21 presents two types of speckle pattern. Photography of these patterns and a subsequent bleaching procedure give specklegrams with smooth (a) and oscillating (b) phase correlation coefficient  $K_\phi$  of the boundary field. The coefficient can be approximated by a function

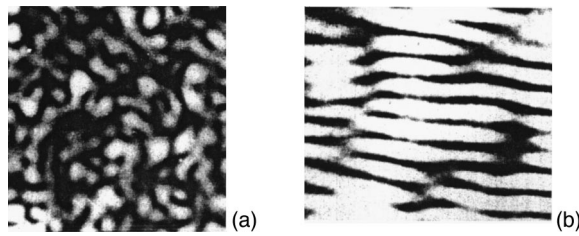


**Fig. 21** Two types of speckle patterns for designing of random plane phase phantoms with smooth (a) and oscillating (b) phase correlation coefficient  $K_\phi$ .

$$K_\phi(\Delta x) = \exp\left[-\left(\frac{|\Delta x|}{l_\phi}\right)^a\right] \cos^2\left(\frac{\pi\Delta x}{2l_0}\right), \quad (18)$$

where  $\Delta x$  is the shift along coordinate  $x$  in specklegram plane,  $l_\phi$  is the phase correlation length of the boundary field,  $l_0$  is the semispacing of the  $K_\phi$  oscillations, and  $a$  is the form factor.

Figure 22 represents the experimental data for evolution of the average intensity fringe contrast along the longitudinal coordinate  $z$ . The phase screen phantom possesses a smooth correlation coefficient  $K_\phi(\Delta x)$ , as well as corresponding theoretical curves calculated using experimental statistical parameters of phantoms. The phase correlation coefficients  $K_\phi(\Delta x)$  reconstructed on the base of experimental data for two types of investigated phantoms are presented in Figure 23. These data show the possibility of estimation of statistical properties of biological phase object using a described spatially resolved technique.

**5.2 PROPAGATION OF THE FOCUSED SPATIALLY MODULATED LASER BEAM**

For a spatially modulated laser beam with parallel interference fringes and spacing  $\Lambda$  focusing of the beam using a diffractively limited optical system

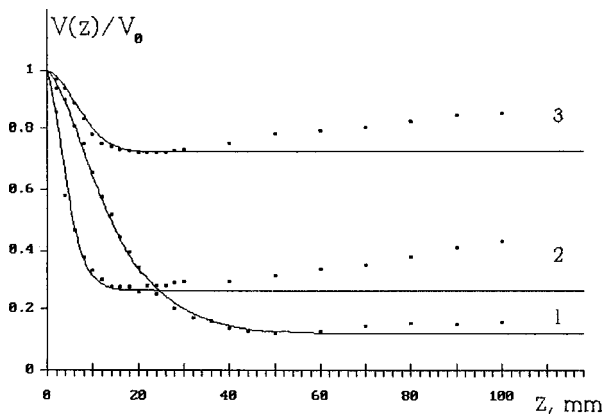


**Fig. 22** Experimental (points) and theoretical (solid lines) plots of relative contrast on distance from the object.  $|\mu(z)| = V(z)/V_0$  for the specklegrams with a smooth correlation coefficient  $K_\phi$ : 1— $\sigma_\phi = 0.625$ ,  $l_\phi = 6.4 \mu\text{m}$ ,  $a = 2.45$ ; 2— $\sigma_\phi = 1.12$ ,  $l_\phi = 7.8 \mu\text{m}$ ,  $a = 2$  (Gaussian shape); 3— $\sigma_\phi = 1.3$ ,  $l_\phi = 5.6 \mu\text{m}$ ,  $a = 2.5$ .

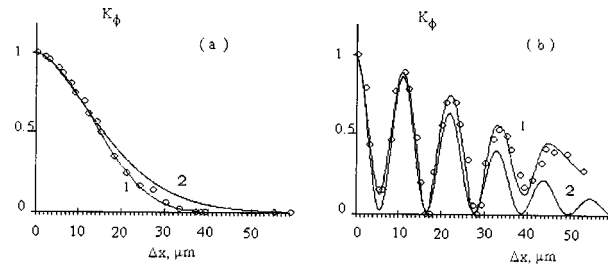


**Fig. 23** Plots of the phase correlation coefficient  $K_\phi$  reconstructed from experimental data (1) and theoretical ones (2), calculated using experimental data, for two types of random phase phantoms.

with an aperture  $D > \Lambda$  gives two spatially isolated light spots in the focusing area (see Figure 24).<sup>118,119</sup> When spots coincide with the scattering object surface in the diffraction field two completely *nonidentical* (noncorrelated) speckle fields are formed, since two different areas of the object are illuminated. If the fringe spacing  $\Lambda < \epsilon_\perp$  (the mean speckle size in the observation plane) and the waist beam diameter  $2w_0 > l_\phi$ , then within separate speckles regular interference fringes are observed whose position changes in a random way when going from one speckle to another. The contrast of the fringes is dictated only by the relationship of intensities of interfering fields, and does not depend on the statistical properties of the object. If  $\Lambda > \epsilon_\perp$  and  $2w_0 > l_\phi$ , no fringes are observed in the scattered field [see Figure 25(b)], but a system of interference fringes of average intensity appears when the object is moved in the transverse direction [see Figure 25(c)]. The contrast of this pattern is defined by the statistical properties of the object.<sup>118,119</sup>

For focused beams the evolution of the average intensity fringe contrast  $V/V_0$  with the distance  $z$  is defined by the difference in beam divergence  $\bar{\theta}$  and  $\tilde{\theta}$  corresponding to nonscattered and scattered field components. The beam divergence fluctuation component depends on the statistical parameters of the boundary field,  $\sigma_\phi$  and  $l_\phi$ . When  $\sigma_\phi$  is not small and  $l_\phi$  is rather large, then the fluctuating component should be great and its divergence equal to the nonscattered one,  $\tilde{\theta} \cong \bar{\theta}$ . Therefore, fringe contrast

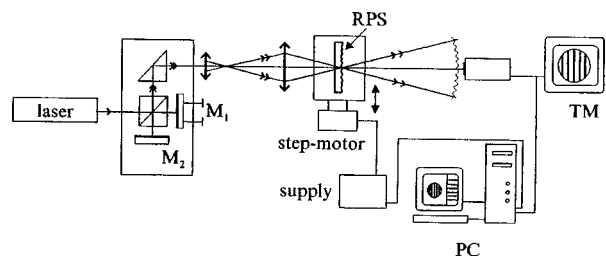


**Fig. 24** Scheme for interference fringe recording in the diffraction field for a focused spatially modulated laser beam transmitted through a random phase object.

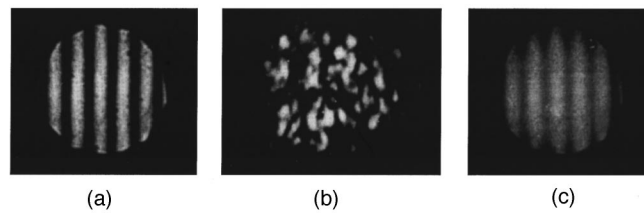


**Fig. 25** The interferograms observed without object (phantom) (a), with stationary (b), and movable (c) object.

should be small with a weak dependence on the distance  $z$ . For the small  $l_\phi$ , when  $\bar{\theta} < \tilde{\theta}$ , due to the space filtering effect relative fringe contrast  $V/V_0$  goes up with distance  $z$ . For the fixed value of  $l_\phi$ ,<sup>118,119</sup>

$$V/V_0 \approx \exp(-\sigma_\phi^2). \quad (19)$$

For rather large  $l_\phi$ , when  $\bar{\theta} \approx \tilde{\theta}$  and  $V_0 < 1$  in this expression, the proportionality changes on approximate equality. The described behavior of  $V/V_0$  on  $z$  is well illustrated by experimental data for plane solid phantoms with different statistical properties.<sup>118,119</sup>

### 5.3 BIOMEDICAL APPLICATIONS

The spatially resolved speckle technique allows one to determine the statistical parameters of biological phase objects, such as standard deviation  $\sigma_\phi$  and correlation length  $l_\phi$  of the boundary field.<sup>119</sup> Theoretical basis of this technique can be applied to the phase objects with rather smooth irregularities and Gaussian statistics. For testing of objects with non-Gaussian statistics or with sharp nonuniformities the technique can be applied as well but calibration is needed. Direct measurements and fast action of the measuring system allow one to use this technique for rapid object inspection. These advantages are very important for biological tissue and cell structure investigations, in particular, for the design of optical topography schemes.<sup>1-3</sup> As well as described in Sec. 2 for the spatial speckle-correlation method, this technique can be used for investigation of thin layers of human skin epidermis, or more thick scleral tissue in its optical clearing process. It has a fine outlook for transparent eye tissue investigation, such as in the cornea and lens.

Besides tissue statistical parameter monitoring the developed approach should be of great use for designing the new generation of laser retinometers, allowing one to measure the retinal visual acuity for the eye with a turbid (cataractous) lens.<sup>115</sup> The scanning of a focused spatially modulated beam will allow a patient to see the interferential fringes in spite of eye lens turbidity, which occurs due to statistical averaging of the speckle modulated pattern.

It is important to note that designed photographic technology for producing the solid-state

plane phantoms may be considered as a technology for the making of a set of special standards of scattering objects. Such scattering standards can be used for calibration of coherent-domain instruments for thin tissue layers and cell structure imaging. A pile of such plane phantoms consequently positioned in the way of a light beam will be a good model for the study of coherent light scattering of the bulk tissue.<sup>99,119</sup>

## 6 CONCLUSION

This article discusses some aspects of speckle optical technologies and their applications to biomedical science. It can be concluded that the theoretical basis of such technologies is satisfactorily developed, that allows one to apply them to many types of tissue layers and cell structures showing single or low step scattering. Many advantages are expected in the field of speckle-polarization effects providing additional selectivity and sensitivity to tissue structure and material anisotropy.<sup>84,85,120,121</sup>

The speckle technique is a very promising instrument for investigation of dynamics of living objects and can be applicable in many areas of medicine like ophthalmology, dermatology, and gastroenterology.<sup>3,12-22,76,96-100</sup>

Actually, it is expected that the most robust instruments for monitoring blood and lymph flow, as well as for tissue motion detection, will be optical designs based on speckle technologies.

Some problems of tissue imaging and topography can be overcome using speckle techniques. Moreover, the speckle phenomenon should be taken into account for many biomedical applications of laser microscopy.<sup>3,37,122</sup> But the problem is to extend speckle technologies to be applicable for thick tissues. Some aspects of solving of this problem for monitoring blood flow and tissue structure can be found in past articles.<sup>53-57,72,84,85,99</sup> The use of low coherence light sources like those used for partially coherent interferometry and tomography (see, for example, Refs. 4, 58-62, 123) seems to be a fruitful approach for tissue structure and dynamics analysis. On the other hand, it was shown recently that the speckle interferometer with sharply focused beams (large numerical aperture of focusing objectives) has a longitudinal resolution up to a few micrometers even for a light source with a high coherence length.<sup>124,125</sup>

## Acknowledgments

The author is grateful to his colleagues and students for their cooperation, especially to Professor V. P. Ryabukho, Professor S. S. Ul'yanov, Professor S. R. Utz, Professor D. A. Zimnyakov, Dr. I. L. Maksimova, Dr. I. L. Kon, and students A. A. Mishin, A. A. Bednov, S. S. Kuz'min, K. V. Larin, and A. A. Chaussky. The research described in this publication was made possible in part by Award N RB1-230 of the U.S. Civilian Research and Development Foundation for the Independent States of the Former Soviet Union (CRDF); by the grant "Leading Scientific Schools" (No. 96-15-96389) of the Russian Basic Research Foundation; and by the individual grants "Soros Professor 1997" (No. 372p), and "Soros Professor 1998" (No. p98-768) of the International Soros Science Education Program (ISSEP).

## REFERENCES

1. *Medical Optical Tomography: Functional Imaging and Monitoring*, G. Mueller, B. Chance, R. Alfano et al., Eds., Vol. IS11, SPIE, Bellingham, WA (1993).
2. *Tissue Optics: Applications in Medical Diagnostics and Therapy*, V. V. Tuchin, Ed., Vol. MS102, SPIE Milestone Series, SPIE, Bellingham, WA (1994).
3. *Coherence-Domain Methods in Biomedical Optics*, V. V. Tuchin, Ed., Vol. 2732, CIS Book of Selected Papers, SPIE, Bellingham, WA (1996).
4. A. F. Fercher, "Optical coherence tomography," *J. Biomed. Opt.* **1**, 157-173 (1996).
5. J. M. Schmitt, A. H. Gandjbakhche, and R. F. Bonner, "Use of polarized light to discriminate short-path photons in a multiply scattering medium," *Appl. Opt.* **31**, 6535-6546 (1992).
6. D. Bicout, C. Brosseau, A. S. Martinez, and J. M. Schmitt, "Depolarization of multiply scattering waves by spherical diffusers: Influence of the size parameter," *Phys. Rev. E* **49**, 1767-1770 (1994).
7. M. R. Ostermeyer, D. V. Stephens, L. Wang, and S. L. Jacques, "Nearfield polarization effects on light propagation in random media," *OSA TOPS Biomed. Opt. Spectrosc. Diagnostics* **3**, 20-25 (1996).
8. A. H. Hielscher, J. R. Mourant, and I. J. Bigio, "Influence of particle size and concentration on the diffuse backscattering of polarized light," *OSA TOPS Biomed. Opt. Spectrosc. Diagnostics* **3**, 26-31 (1996).
9. H. Horinaka, K. Hashimoto, K. Wada, and Y. Cho, "Extraction of quasi-straightforward-propagating photons from diffused light transmitting through a scattering medium by polarization modulation," *Opt. Lett.* **20**, 1501-1503 (1995).
10. J. F. de Boer, T. E. Milner, M. J. C. van Gemert, and J. S. Nelson, "Two-dimensional birefringence imaging in biological tissue by polarization-sensitive optical coherence tomography," *Opt. Lett.* **22**, 934-936 (1997).
11. S. P. Morgan, M. P. Khong, and M. G. Somekh, "Effects of polarization state and scatterer concentration on optical imaging through scattering media," *Appl. Opt.* **36**, 1560-1565 (1997).
12. O. J. Lokberg, "Speckles and speckle techniques for biomedical applications," *Proc. SPIE* **1524**, 35-47 (1991).
13. J. D. Briers, "Monitoring biomedical motion and flow by means of coherent light fluctuations," *Proc. SPIE* **2732**, 2-15 (1996).
14. J. D. Briers and S. Webster, "Laser speckle contrast analysis (LASCA): A non-scanning, full-field technique for monitoring capillary blood flow," *J. Biomed. Opt.* **1**, 174-179 (1996).
15. J. D. Briers, "Laser Doppler and time-varying speckle: A reconciliation," *J. Opt. Soc. Am. A* **13**, 345-350 (1996).
16. Y. Aizu and T. Asakura, "Biospeckle phenomena and their application to the evaluation of blood flow," *Opt. Laser Technol.* **23**, 205-219 (1991).
17. Y. Aizu et al., "Evaluation of blood flow at ocular fundus by using laser speckle," *Appl. Opt.* **31**, 3020-3029 (1992).
18. B. Ruth, "Blood flow determination by the laser speckle method," *Int. J. Microcirc.: Clin. Exp.* **9**, 21-45 (1990).
19. B. Ruth, "Measuring the steady-state value and the dynamics of the skin blood flow using the noncontact laser method," *Med. Biol. Eng. Comput.* **16**, 105-111 (1994).
20. H. Fujii, "Visualization of retinal blood flow by laser speckle flowgraphy," *Med. Biol. Eng. Comput.* **32**, 302-304 (1994).
21. N. Konishi and H. Fujii, "Real-time visualization of retinal microcirculation by laser flowgraphy," *Opt. Eng.* **34**, 753-757 (1995).
22. B. Zang, C. M. Pleass, and C. S. Ih, "Feature information extraction from dynamic biospeckle," *Appl. Opt.* **33**, 231-237 (1994).
23. E. Leith et al., "Electronic holography and speckle methods for imaging through tissue using femtosecond gated pulses," *Appl. Opt.* **30**, 4204-4210 (1991).
24. P. Naulleau, D. Dilworth, E. Leith, and J. Lopez, "Resolution-enhanced detection of moving objects embedded within scattering media using time-gated speckle methods," *Appl. Opt.* **35**, 3065-3067 (1996).
25. H. S. Dhadwal, R. R. Ansari, and M. A. Della Vecchia, "Coherent fiber optic sensor for early detection of cataractogenesis in a human eye lens," *Opt. Eng.* **32**, 233-238 (1993).
26. M. Dieckman and K. Dierks, "Diagnostics methods and tissue parameter investigations together with measurement results (*in vivo*)," *Proc. SPIE* **2126**, 331-345 (1994).
27. K. Wardell, I. M. Braverman, D. G. Silverman, and G. E. Nilsson, "Spatial heterogeneity in normal skin perfusion recorded with laser Doppler imaging and flowmetry," *Microvasc. Res.* **48**, 26-38 (1994).
28. A. P. Shepherd and P. A. Oberg, *Laser Doppler Blood Flowmetry*, Kluwer, Boston (1990).
29. M. H. Koelink et al., "Laser Doppler blood flowmetry using two wavelengths: Monte Carlo simulations and measurements," *Appl. Opt.* **33**, 3549-3556 (1994).
30. T. J. H. Essex and P. O. Byrne, "A laser Doppler scanner for imaging blood flow in skin," *J. Biomed. Eng.* **13**, 189-194 (1991).
31. C. E. Riva, B. L. Petring, R. D. Shonat, and C. J. Pournaras, "Scattering process in LDV from retinal vessels," *Appl. Opt.* **28**, 1078-1083 (1989).
32. E. R. Ingofsson, L. Tronstad, E. V. Hersh, and C. E. Riva, "Efficacy of laser Doppler flowmetry in determining pulp vitality of human teeth," *Endod. Dent. Traumatol.* **10**, 83-87 (1994).
33. De Yu Zang, P. Wilder-Smith, J. E. Millerd, and A. M. A. Arrastia, "Novel approach to laser Doppler measurement of pulpal blood flow," *J. Biomed. Opt.* **2**, 304-309 (1997).
34. S. M. Khanna et al., "Cellular vibration and motility in the organ of corti," *Acta Oto-Laryngol. Suppl.* **467**, 1-279 (1989).
35. N. Stasche et al., "Middle ear transmission disorders tympanic membrane vibration analysis by laser-Doppler vibrometry," *Acta Oto-Laryngol.* **114**, 59-63 (1994).
36. J. R. Zipp and J. J. ten Bosch, "Two-dimensional patterns of Fraunhofer diffraction by dental enamel," *Proc. SPIE* **2626**, 14 (1995).
37. B. R. Masters, "Fourier transform analysis to evaluate human corneal endothelial cells," *Proc. SPIE* **2732**, 144-154 (1996).
38. L. Poupinet and G. Jarry, "Heterodyne detection for measuring extinction coefficient in mammalian tissue," *J. Opt. (Paris)* **24**, 279-285 (1993).
39. M. Kempe, W. Rudolph, and E. Welsch, "Comparative study of confocal and heterodyne microscopy for imaging through scattering media," *J. Opt. Soc. Am. A* **13**, 46-52 (1996).
40. B. Devaraj, M. Usa, K. P. Chan, T. Akatsuka, and H. Inaba, "Recent advances in coherent detection imaging (CDI) in biomedicine. Lasertomography of human tissue *in vivo* and *in vitro*," *IEEE J. Sel. Top. Quantum Electron.* **2**, 1008-1016 (1996).
41. A. Wax and J. E. Thomas, "Optical heterodyne imaging and

- Wigner phase space distributions," *Opt. Lett.* **21**, 1427–1429 (1996).
42. V. Tychinsky et al., "Optical phase images of living micro objects," *Proc. SPIE* **2100**, 129–136 (1994).
  43. V. P. Tychinsky, "Microscopy of subwave structures," *Usp. Fiz. Nauk* **166**, 1219–1229 (1996).
  44. *Handbook of Biological Confocal Microscopy*, J. B. Pawley, Ed., Plenum, New York (1990).
  45. *Confocal Microscopy*, B. R. Masters, Ed., Vol. MS131, SPIE Milestone Series, SPIE, Bellingham, WA (1996).
  46. *Confocal Microscopy*, T. Wilson, Ed., Academic, London (1990).
  47. T. F. Watson, "Application of high-speed confocal imaging techniques in operative dentistry," *Scanning* **16**, 168–173 (1994).
  48. B. R. Masters and A. A. Thaeer, "Real time scanning slit confocal microscopy of the *in vivo* human cornea," *Appl. Opt.* **33**, 695–701 (1994).
  49. M. Rajadhyaksha, M. Grossman, D. Esterowitz, R. H. Webb, and R. R. Anderson, "In vivo confocal scanning laser microscopy of human skin: melanin provides strong contrast," *J. Invest. Dermatol.* **104**, 946–952 (1995).
  50. V. B. Karpov, "Study of biological samples with a laser Fourier holographic microscopy," *Laser Phys.* **4**, 618–623 (1994).
  51. S. C. W. Hyde, N. P. Barry, R. Jones, J. C. Dainty, and P. M. W. French, "Sub-100 pm depth-resolution holographic imaging through scattering media in the near infrared," *Opt. Lett.* **20**, 2320–2322 (1996).
  52. E. Beaupaire, A. C. Boccara, M. Lebec, L. Blanchot, and H. Saint-Jalmes, "Full-field optical coherence microscopy," *Opt. Lett.* **23**, 244–246 (1998).
  53. M. H. Kao, A. G. Yodh, and D. J. Pine, "Observation of Brownian motion on the time scale of hydrodynamic interactions," *Phys. Rev. Lett.* **70**, 242–245 (1993).
  54. P. D. Kaplan, A. D. Dinsmore, A. G. Yodh, and D. J. Pine, "Diffuse-transmission spectroscopy: a structural probe of opaque colloidal mixtures," *Phys. Rev. E* **50**, 4827–4835 (1994).
  55. D. A. Boas, L. E. Campbell, and A. G. Yodh, "Scattering and imaging with diffusing temporal field correlations," *Phys. Rev. Lett.* **75**, 1855–1858 (1995).
  56. D. A. Boas et al., "Diffusion of temporal field correlation with selected applications," *Proc. SPIE* **2732**, 34–46 (1996).
  57. A. G. Yodh and N. Georgiades, "Diffusing-wave interferometry," *Opt. Commun.* **83**, 56–59 (1991).
  58. A. F. Fercher, C. K. Hitzenberger, and W. Drexler, "Ocular partial-coherence interferometry," *Proc. SPIE* **2732**, 210–228 (1996).
  59. F. Fercher, W. Drexler, and C. K. Hitzenberger, "Ocular partial-coherence tomography," *Proc. SPIE* **2732**, 229–241 (1996).
  60. *Coherence Domain Methods in Biomedical Science and Clinical Applications*, V. V. Tuchin, H. Podbielska, and B. Ovaryn, Eds., Vol. 2981, SPIE, Bellingham, WA (1997).
  61. *Coherence Domain Methods in Biomedical Science and Clinical Applications II*, V. V. Tuchin and J. A. Izatt, Eds., Vol. 3251, SPIE, Bellingham, WA (1998).
  62. J. A. Izatt, M. D. Kulkarni, K. Kobayashi, M. V. Sivak, J. K. Barton, and A. J. Welch, "Optical coherence tomography for biagnostics," *Opt. Photonics News* **8**, 41–65 (1997).
  63. R. G. Johnston, S. B. Singham, and G. C. Salzman, "Polarized light scattering," *Comm. Mol. Cell. Biophys.* **5**, 171–192 (1988).
  64. G. C. Salzman, S. B. Singham, R. G. Johnston, and C. F. Bohren, "Light scattering and cytometry," in *Flow Cytometry and Sorting*, pp. 81–107, Wiley-Liss, New York (1990).
  65. B. V. Bronk, S. D. Druger, J. Czege, and W. van de Merve, "Measuring diameters of rod-shaped bacteria *in vivo* with polarized light scattering," *Biophys. J.* **69**, 1170–1177 (1995).
  66. A. W. Dreher and K. Reiter, "Polarization technique measures retinal nerve fibers," *Biomed. Opt. (Newsletter)* **1**(3), 1 (1992).
  67. V. V. Tuchin, "Light scattering study of tissues," *Usp. Fiz. Nauk* **167**, 517–539 (1997).
  68. V. V. Tuchin, "Coherence-domain methods in tissue and cell optics," *Laser Phys.* **8**, 807–849 (1998).
  69. S. M. Rhytov, Yu. A. Kravtsov, and V. I. Tatarsky, *Introduction to Statistical Radiophysics, Pt. 2, Random Fields*, Nauka, Moscow (1978).
  70. J. W. Goodman, *Statistical Optics*, Wiley, New York (1985).
  71. E. L. Church, "Fractal surface finish," *Appl. Opt.* **27**, 1518–1526 (1988).
  72. R. Berkovits and S. Feng, "Theory of speckle-pattern tomography in multiple-scattering media," *Phys. Rev. Lett.* **65**, 3120–3123 (1990).
  73. D. A. Zimnyakov and V. V. Tuchin, "Fractality of speckle intensity fluctuations," *Appl. Opt.* **35**, 4325–4333 (1996).
  74. D. A. Zimnyakov, V. V. Tuchin, and A. A. Mishin, "Visualization of biotissue fractal structures using spatial speckle-correlometry method," *Izvestiya VUIZ, Appl. Nonlinear Dyn.* **4**, 49–58 (1996).
  75. D. A. Zimnyakov, V. V. Tuchin, and S. R. Utz, "Investigation of statistical properties of partly developed speckle fields in application to skin structure diagnostics," *Opt. Spectrosc.* **76**, 838–844 (1994).
  76. S. S. Ul'yanov, D. A. Zimnyakov, and V. V. Tuchin, "Fundamentals and applications of dynamic speckles induced by focused laser beam scattering," *Opt. Eng.* **33**, 3179–3201 (1994).
  77. D. A. Zimnyakov, V. V. Tuchin, S. R. Utz, and A. A. Mishin, "Speckle imaging methods using focused laser beams in applications to tissue mapping," *Proc. SPIE* **2433**, 411–420 (1995).
  78. D. A. Zimnyakov and V. V. Tuchin, "About two modality of speckle intensity distributions for large-scale phase scatterers," *Lett. J. Tech. Phys.* **21**, 10–14 (1995).
  79. D. A. Zimnyakov and V. V. Tuchin, "Lens-like local scatterers approach to the biotissue structure analysis," *Proc. SPIE* **2647**, 334–342 (1995).
  80. D. A. Zimnyakov, V. P. Ryabukho, and K. V. Larin, "Micro-lens effect manifestation in focused beam diffraction on large scale phase screens," *Lett. J. Tech. Phys.* **20**, 14–19 (1994).
  81. D. A. Zimnyakov, "Scale effects in partially developed speckle structure. The case of Gaussian phase screens," *Opt. Spectrosc.* **79**, 155–162 (1995).
  82. V. V. Tuchin, S. R. Utz, and I. V. Yaroslavsky, "Tissue optics, light distribution, and spectroscopy," *Opt. Eng.* **33**, 3178–3188 (1994).
  83. *Laser Speckle and Related Phenomena*, J. C. Dainty, Ed., Springer-Verlag, Berlin (1975).
  84. D. A. Zimnyakov, V. V. Tuchin, and A. A. Mishin, "Spatial speckle correlometry in applications to tissue structure monitoring," *Appl. Opt.* **36**, 5594–5607 (1997).
  85. V. V. Tuchin et al., "Light propagation in tissues with controlled optical properties," *J. Biomed. Opt.* **2**(4), 401–417 (1997).
  86. V. V. Bakutkin et al., "Light scattering of human eye sclera," *Appl. Spectroscopy (USSR)* **46**(1), 104–107 (1987).
  87. P. O. Rol, *Optics for Transscleral Laser Application*, Doctoral Dissertation, Institute of Biomedical Engineering, Zurich, Switzerland (1992).
  88. J. S. Maier et al., "Possible correlation between blood glucose concentration and the reduced scattering coefficient of tissue in the near infrared," *Opt. Lett.* **19**, 2062–2064 (1994).
  89. M. Kohl, M. Cope, M. Essenpreis, and D. Bocker, "Influence of glucose concentration on light scattering in tissue-simulating phantoms," *Opt. Lett.* **19**, 2170–2172 (1994).
  90. H. Lui, B. Beauvoit, M. Kimura, and B. Chance, "Dependence of tissue optical properties on solute-induced changes in refractive index and osmolarity," *J. Biomed. Opt.* **1**, 200–211 (1996).
  91. B. Grzegorzewski and S. Yermolenko, "Speckles in far-field produced by fluctuations associated with phase separation," *Proc. SPIE* **2647**, 343–349 (1995).
  92. J. T. Bruulsema et al., "Correlation between blood glucose concentration in diabetics and noninvasively measured tissue optical scattering coefficient," *Opt. Lett.* **22**, 190–192 (1997).
  93. A. Kotyk and K. Janacek, *Membrane Transport: an Interdisciplinary Approach*, Plenum, New York (1977).

94. *Tables of Physical Constants, Handbook*, I. K. Kikoin, Ed., Atomizdat, Moscow (1976).
95. D. A. Zimnykov, V. V. Tuchin, and K. V. Larin, "Speckle patterns polarization analysis as an approach to turbid tissues structure monitoring," *Proc. SPIE* **2981**, 172–180 (1997).
96. S. S. Ul'yanov, "New type of manifestation of the Doppler effect: an application to blood and lymph flow measurements," *Opt. Eng.* **34**, 2850–2855 (1995).
97. S. S. Ul'yanov et al., "The application of speckle-interferometry method for the monitoring of blood and lymph flow in microvessels," *Lasers Med. Sci.* **11**, 97–107 (1996).
98. A. A. Bednov, S. S. Ulyanov, V. V. Tuchin, G. E. Brill, and E. I. Zakharova, "Investigation of lymph flow dynamics by speckle-interferometry method," *Izvestiya VUZ, Appl. Non-linear Dyn.* **4**(3), 42–51 (1996) (in Russian); English translation: *Proc. SPIE* **3177**, 89–96 (1997).
99. S. S. Ulyanov, "Speckled speckle statistics with a small number of scatterers: implication for blood flow measurement," *J. Biomed. Opt.* **3**, 237–245 (1998).
100. T. Yamamoto and T. Asakura, "Noninvasive evaluation of the retinal blood circulation using laser speckle phenomena," *J. Clinical Laser Med. Surg.* **8**(5), 35–45 (1990).
101. M. Henning, D. Gerdt, and T. Spraggins, "Using a fiber-optic pulse sensor in magnetic resonance imaging," *Proc. SPIE* **1420**, 34–40 (1991).
102. S. M. Khanna et al., "A noninvasive optical system for the study of the function of inner ear in living animals," *Proc. SPIE* **2732**, 64–81 (1996).
103. M. Maeta, S. Kawakami, T. Ogawara, and Y. Masuda, "Vibration analysis of the tympanic membrane with a ventilation tube and a perforation by holography," *Proc. SPIE* **1429**, 152–161 (1991).
104. G. Dacosta, "Optical remote sensing of heartbeats," *Opt. Commun.* **117**, 395–398 (1995).
105. V. Tuchin et al., "Laser speckle and optical fiber sensors for micromovements monitoring in biotissues," *Proc. SPIE* **1420**, 81–92 (1991).
106. S. S. Ulyanov, V. P. Ryabukho, and V. V. Tuchin, "Speckle-fields interference for biotissue vibrations measurements," *Opt. Eng.* **33**, 908–914 (1994).
107. S. Yu. Kuzmin, S. S. Ul'yanov, V. V. Tuchin, and V. P. Ryabukho, "Speckle and speckle-interferometric methods in cardiognostics," *Proc. SPIE* **2732**, 82–99 (1996).
108. M. Conerty et al., "Development of otolaryngological interferometric fiber optic diagnostic probe," *Proc. SPIE* **1649**, 98–105 (1992).
109. V. M. Aranchuk and N. N. Zatsepin, "On Doppler speckle-interferometer signal amplitude dependence upon relation between speckle-sizes and receiving aperture," *J. Tech. Phys.* **58**, 2060–2062 (1988).
110. S. S. Ul'yanov and V. V. Tuchin, "The analysis of space-time projection of differential and Michelson-type output signal for measurement," *Proc. SPIE* **1981**, 165–174 (1992).
111. I. A. Popov, "Spectrum of Doppler shifts of coherent radiation scattered by oscillating rough surface," *Sov. J. Opt. Technol.* **N11**, 48–53 (1994).
112. R. W. Wygant, S. P. Almeida, and O. D. D. Scars, "Surface inspection via projection interferometry," *Appl. Opt.* **27**, 4626–4630 (1988).
113. R. Jones and C. Wykes, *Holographic and Speckle Interferometry*, Cambridge University Press, Cambridge (1983).
114. G. R. Lokshin, S. M. Kozel, I. S. Klimenko, and V. E. Belonuchkin, "Modulation methods in holographic interferometry," *Opt. Spectrosc.* **72**(6), 1444–1450 (1992).
115. A. V. Priezzhev, V. V. Tuchin, and L. P. Shubochkin, *Laser Diagnostics in Biology and Medicine*, Nauka, Moscow (1989).
116. V. P. Ryabukho et al., "Correlation effects of diffraction speckle-fields of spatially-modulated laser beam on random phase screen," *Lett. J. Tech. Phys.* **20**(11), 74–78 (1994).
117. V. P. Ryabukho and A. A. Chaussky, "Speckle-fields interference in zone of diffraction of focused spatially modulated laser beam on a random phase screen," *Lett. J. Techn. Phys.* **21**(16), 57–62 (1995).
118. V. P. Ryabukho, A. A. Chaussky, and V. V. Tuchin, "Interferometric testing of the random phase objects by focused spatially modulated laser beam," *Photonics Optoelectron.* **3**, 77–85 (1995).
119. V. P. Ryabukho et al., "Interferometric testing of the random phase objects (biological tissue models) by spatially modulated laser beam," *Proc. SPIE* **2732**, 100–117 (1996).
120. I. Freund, M. Kaveh, R. Berkovits, and M. Rosenbluh, "Universal polarization correlations and microstatistics of optical waves in random media," *Phys. Rev. B* **42**, 2613–2616 (1990).
121. A. G. Ushenko, S. V. Ermolenko, and M. A. Neduzhko, "About rough surfaces light scattering matrices correlation microstructure," *Opt. Spectrosc.* **69**, 1099–1105 (1990).
122. J. M. Schmitt and A. Knüttel, "Model of optical coherence tomography of heterogeneous tissue," *J. Opt. Soc. Am. A* **14**, 1231–1242 (1997).
123. G. Häusler, J. M. Herrmann, R. Kummer, and M. W. Linder, "Observation of light propagation in volume scatterers with  $10^{11}$ -fold slow motion," *Opt. Lett.* **21**, 1087–1089 (1996).
124. V. P. Ryabukho, V. L. Khomutov, D. V. Lyakin, and K. V. Konstantinov, "Laser interferometer with sharply focused beams for monitoring of an object displacement," *Lett. J. Tech. Phys.* **23**, 116–117 (1997).
125. V. P. Ryabukho, V. L. Khomutov, V. V. Tuchin, D. V. Lyakin, and K. V. Konstantinov, "Laser interferometer with an object sharply focused beam as a tool for optical tomography," *Proc. SPIE* **3251**, 247–252 (1998).